Norwegian University of Life Sciences
Faculty of Environmental Science and Technology
Department of Mathematical Sciences and Technology

Master Thesis 2015
30 credits

Use of the Resonance Structure of Mie Scattering for Refractive Index Estimation

Bruk av resonansstrukturen til Mie-spredning for estimering av brytningsindeks

Nora Klevjer Thøgersen

Acknowledgements

This thesis is the fulfillment of my Master's degree at the Norwegian University of Life Sciences (NMBU).

I would like to thank my supervisors, Prof. Achim Kohler and Prof. Arkadi Ponossov and Dr. Rozalia Lukacs for guidance and advice. I would like to express my gratitude to Nicolay and Oscar, for their help in reading and correcting my terrible grammatical errors.

I would also like to thank my friends for many awesome years at NMBU; Solveig, Siri, Nina, Testin, Stine and Karen Marie. These six years would not have been the same without you. Big thanks to my fellow students at TF211 for keeping me company during late nights. Especially Solveig for advice, for being a great friend and for many fun lunches.

Finally, yet importantly, I would like to thank my parents for all their support.

Ås, May 15, 2015

Nora Klevjer Thøgersen

Abstract

The Mie extinction for the scattering of infrared light of spherical particles shows both broad background oscillations and resonant structures. The resonance structure, also called ripples, is due to resonant electric and magnetic modes. In this thesis it was evaluated to what extent the ripples in the extinction efficiency can be used to estimate a dispersive real refractive index in the infrared region. In this context, approximation formulas that estimate the distance between ripples in the Mie extinction were of special interest. Different aspects, such as resolution, formula accuracy, resonance order, and resonance index were taken into account when evaluating these formulas.

During the work with this thesis, it was observed that the resolution has a strong effect on the resonance structure. The resolution affects both the shape of the ripple structure, as well as the sharpness and number of visible peaks. It also determines whether first or higher order peaks cause the peaks in the ripple structure. Further, it was found that the choice of formula, for obtaining the best accuracy, depends on resolution.

Sammendrag

Mie-ekstinsjonen til en sfærisk partikkel som blir truffet av infallende infrarødt lys, viser store underliggende oscillasjoner med en overlagret resonansstruktur. Denne resonansstrukturen kalles også ripples, og skyldes resonante elektriske og magnetiske moder. I denne oppgaven ble det evaluert i hvilken grad resonansstrukturen kan brukes til å estimere en dispersiv reell brytningsindeks i det infrarøde området. I den forbindelse var tilærmingsformler for beregning av avstanden mellom disse resonansene av spesiell interesse. Underveis i prosessen ble forskjellige aspekter som oppløsning, tilnærmingsformlene nøyaktighet og resonanseorden og indeks tatt i betrakting.

I løpet av arbeidet med denne oppgaven ble det observert at oppløsningen har en sterk effekt på resonansstrukturen, både når det gjelder form, antall synlige topper og hvor skarpe toppene er. I tillegg har oppløsningen en effekt på hvilken orden det er på resonansene som er synlige i resonansstrukturen. Videre ble det funnet at oppløsningen har innvirkning på hvilken av tilnærmingsformlene for avstanden mellom toppene i resonansstrukturen som gir best resultat.

Contents

Notation

	Notation
Extended Multiplicative Signal Correction	EMSC
Resonant Mie Scattering	RMieS
Fourier Transform IR	FTIR
Extinction efficiency	Q_{ext}
Size parameter	x
Refractive index	m
Radius of the sphere	a
Magnetic mode	b_n
Electric mode	a_n
Sum of the electromagnetic modes	$\sum a_n$
Index or number of resonance	n
Resolution in the wavenumber	$\Delta\tilde{\nu}$
Resolution in the size parameter	Δx
Distance between the peaks	dx

Chapter 1

Introduction

In infrared (IR) spectroscopy of biological material, the aim is to obtain a scatter-free absorbance spectrum with chemically interpretable spectral bands. In biomedical IR spectroscopy it is often desirable to obtain spectra at cellular level. Since cells are strong scatters of infrared radiation they are not well suited for such analysis. These spectra are often distorted by scattering which can make the biochemical information unreliable. IR spectroscopy is potentially a powerful tool, but, for it to be successful, it must be possible to extract reliably a pure absorbance spectra [2, 4, 1].

Gustav Mie published the theory describing analytically the scattering of light from homogeneous spherical particles, later refereed to as Mie theory, in 1908 [11]. In 1957, van de Hulst published an approximation formula for the extinction efficiency Q_{ext}, which did not include spherical Bessel and Hankel functions and therefore required much less computational effort and power [16]. In 2005, Mohlenhoff et al. [12] observed spectra of cells in IR spectroscopy that did not obey Beer-Lambert's law. A scattering background with superimposed absorption features was observed. They showed that this scattering background can be described using the Mie theory of scattering spheres. Kohler et al. managed in 2008 to correct the Mie type scattering oscillations in the baseline using Extended Multiplicative Signal Correction (EMSC) and Principal Component Analysis (PCA) on Fourier transform infrared (FTIR) synchrotron spectra of single lung cancer cells [9]. The so-called "dispersion artifact" remained uncorrected. In 2009, Bassan et al. [1] managed to describe the origin of the "dispersion artifact". This artifact was due to rapid changes in the scattering efficiency at the absorption band, i.e. resonant Mie scattering (RMieS). After understanding the origin of the "dispersion artifact", a new correcting algorithm, which removed both the broad background oscillation and the "dispersion artifact", was constructed [3]. Bassan et al.[4] continued developing this algorithm, and in 2010 they presented

an iterative RMieS-EMSC algorithm which incorporated the full Mie theory.

A method for recovering the complex refractive index from materials with spherical shape was suggested by van Djik et al. in 2013 [17]. This method was in 2015 further developed by Lukacs et al. [10]. It was tested on FTIR synchrotron spectra of PMMA spheres and pollen (approximately spherically shaped). Pure absorbance spectra was obtained for PMMA spheres and the imaginary part of the refractive index was successfully recovered for both PMMA and pollen. In FTIR spectra of a PMMA sphere, the first experimental observation of Mie ripples, was observed.

The aim of this thesis was to determine to what extend the ripples in the extinction efficiency can be used for determination of the refractive index for various materials in the infrared region of light. Petr Chỳlek suggested two formulas for the approximation of the distance between the peaks in the ripple structure of the Mie scattering as a function of the refractive index [6, 7]. Since, in infrared microspectroscopy, spectra of small spheres, i.e. with sizes in the same order as the wavelength of the infrared light, can be obtained, these approximation formulas could be used for the estimation of the refractive index in the infrared region of the electromagnetic spectrum. Petr Chỳlek's approximation formulas are together with bisection used to find an estimate of the refractive index from simulated spectra. During this project, the following has been discovered: The resolution has a strong effect on the resonance structure. It affects both the shape of the ripple structure, the number of visible peaks, and the sharpness of the peaks. Further, it has an impact on if first order or higher order peaks are visible in the ripple structure. It was then determined that the resolution of the simulated spectra has an impact on which of the approximation formulas that should be used. The calculated distance between the resonances from the simulated spectra are compared to the results from the approximation formulas for different refractive indices.

The next chapter (chapter 2), gives a short introduction to FTIR spectroscopy where spectra of the extinction efficiency and from PMMA spheres are shown. Some basic properties are defined before a short summary of the Mie theory is given. The ripple structure is illustrated and the resonances described before the approximation formulas for the distance between the resonances are presented. In chapter 3 the results from exploring the effects of the resolution on Q_{ext}, $\mathsf{a_n}$ and $\sum \mathsf{a_n}$ are displayed. The accuracy of the equations for calculating the distance between the resonances is discussed in addition to the possibility of using these equations for estimating the refractive index. The effects of the resolution on the resonance structure are discussed further in chapter 4. In appendix A an

overview of the Bessel functions is presented and a more detailed description of the Mie coefficients is given in appendix B. In appendix C the numerical results from chapter 3.2.1 are given.

Chapter 2

Theory

2.1 FTIR Spectroscopy

Fourier transform infrared (FTIR) spectroscopy is a biophysical technique for the investigation of biological tissues and cells in their native state. Physical and chemical light are normally distinctc but this is not the case in FTIR spectra. In FTIR spectra the scattering effects from physical and chemical light often overlap. Thus for biochemical interpretation, correction of various types of light scattering effects is desired. Since cells and tissue structures vary on scales comparable to the wavelength of the infrared light, infrared absorbance spectra are often hampered by strong scattering effects [9, 10]. As model systems for characterization of scattering phenomenon, Lukacs et al. [10] used pollen grains and polymethyl methacrylate (PMMA) spheres. PMMA spheres are used as a simple experimental model system to model scattering from cells. Even though their chemical composition is identical, their IR spectra are different. The only factor that can impact the spectra, since their composition are the same, are the physical size of the spheres. Both Mie scattering and the "dispersion artifact", which is explained by the Mie theory, are evident in spectra from the spheres [1].

Pollen grains are an ideal real-world model system for scattering of biological samples because their grain walls are thick and shape resistant. In other words, their morphology is stable and reproducible. This enables simple manipulation and measurement. In addition, the variety of pollen morphologies creates a wide range of experimental conditions for the measurement of scattering [10].

Next, to illustrate how spectra of PMMA spheres change when the diameter is changed, the extinction efficiency for three spheres with different diameter are shown. Data is obtained from Dr. Rozalia Lukacs, Postdoc at NMBU[8]. A PMMA sphere with diameter 40μm is shown in figure 2.1. The resolution is in this spectra $\Delta\tilde{\nu} = 4\text{cm}^{-1}$. The area $56 < x < 90$ is zoomed in on in figure 2.2

to show the fine ripple structure. The two next figures are plotted with higher resolution, $\Delta\tilde{\nu} = 2\text{cm}^{-1}$, and the spectra have a sharper ripple structure than in the previous figures. The extinction efficiency for a PMMA sphere with diameter 15μm is shown in figure 2.3 and figure 2.4. This change in the shape that is visible between the previous figures makes it interesting to explore how the resolution affects the ripple structure. Lukacs et al. recorded samples with $\Delta\tilde{\nu} = 4\text{cm}^{-1}$, so using $\Delta\tilde{\nu} = 5\text{cm}^{-1}$ can make the results comparable to experimental results [10]. In figure 2.5, the absorbance, A, of a sphere with diameter 15μm is plotted. Data for this spectra is obtained from Dr. Rozalia Lukacs, Postdoc at NMBU[8]. In this spectra the scattering effects cancels each other out and therefore the spectra have a flat baseline with no large oscillations.

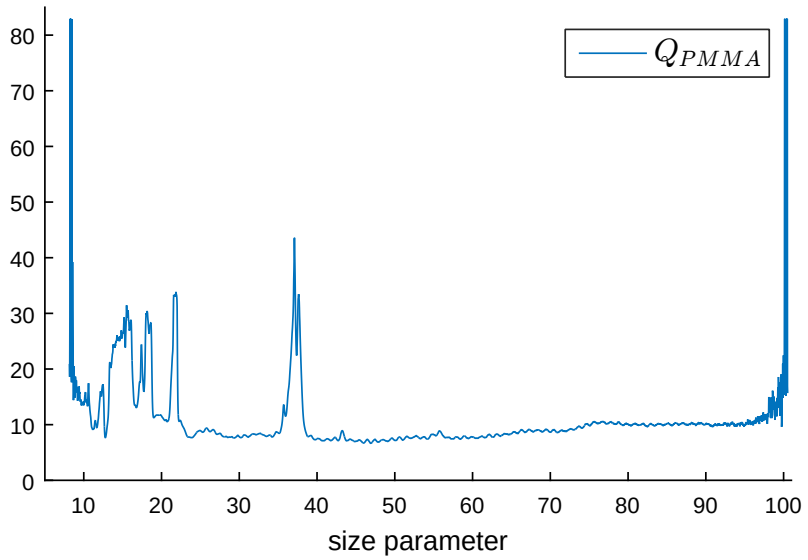

Figure 2.1: Example of spectra from a PMMA sphere plotted with resolution $\Delta\tilde{\nu} = 4\text{cm}^{-1}$ and diameter 40μm.

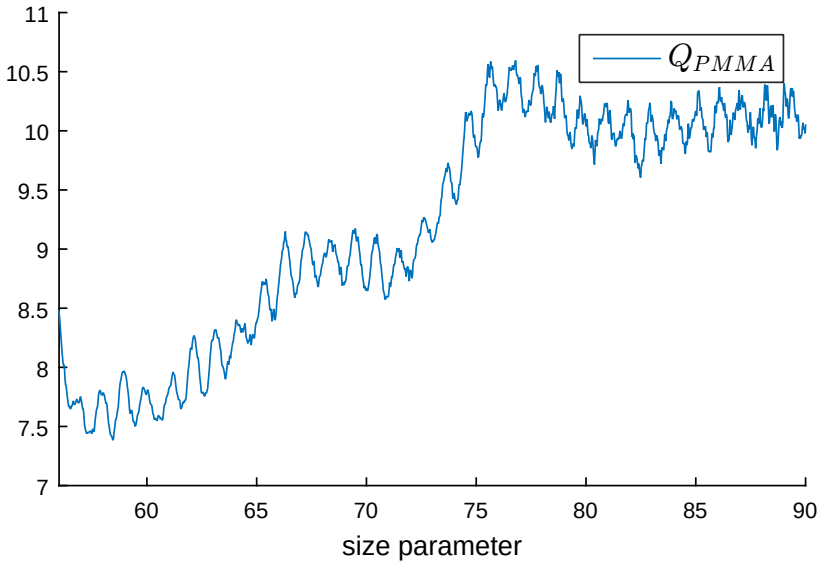

Figure 2.2: Zoomed in on spectra from a PMMA sphere plotted with resolution $\Delta\tilde{\nu} = 4\text{cm}^{-1}$ and diameter 40μm.

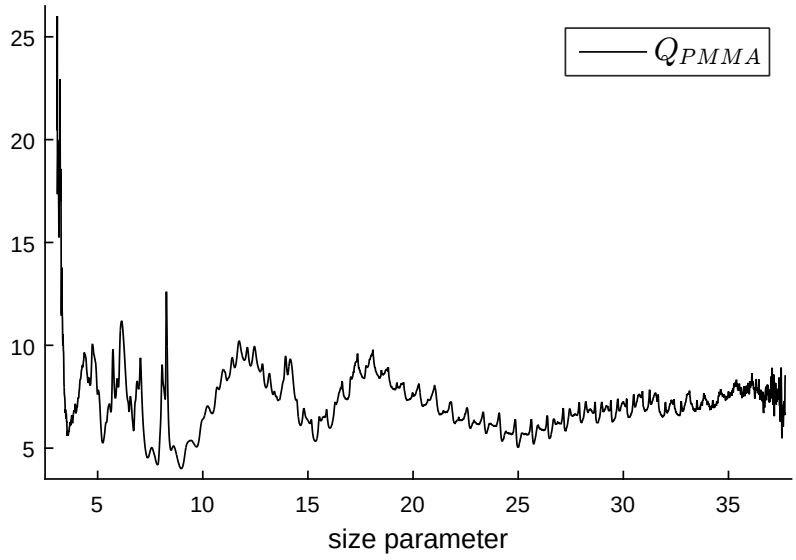

Figure 2.3: Example of spectra from a PMMA sphere plotted with resolution $\Delta\tilde{\nu} = 2\text{cm}^{-1}$ and diameter 15μm.

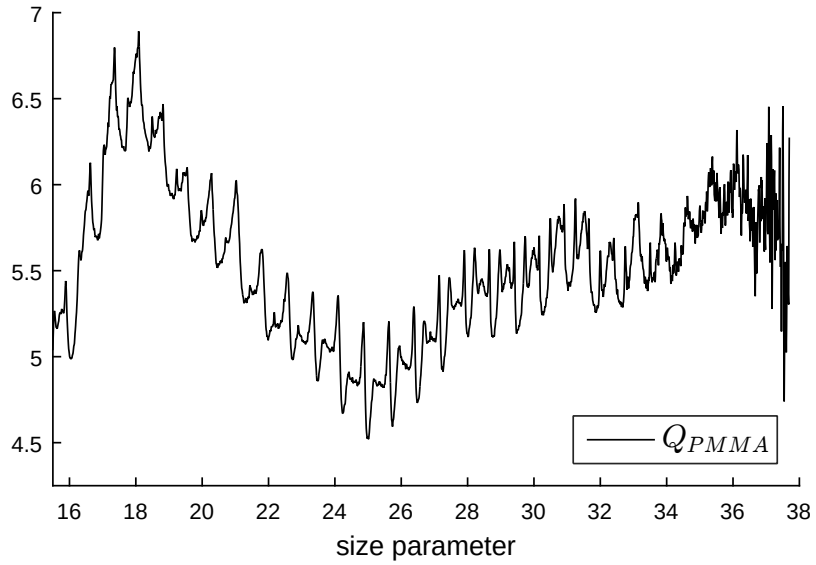

Figure 2.4: Zoomed in on spectra from a PMMA sphere plotted with resolution $\Delta\tilde{\nu} = 2\text{cm}^{-1}$ and diameter 15μm.

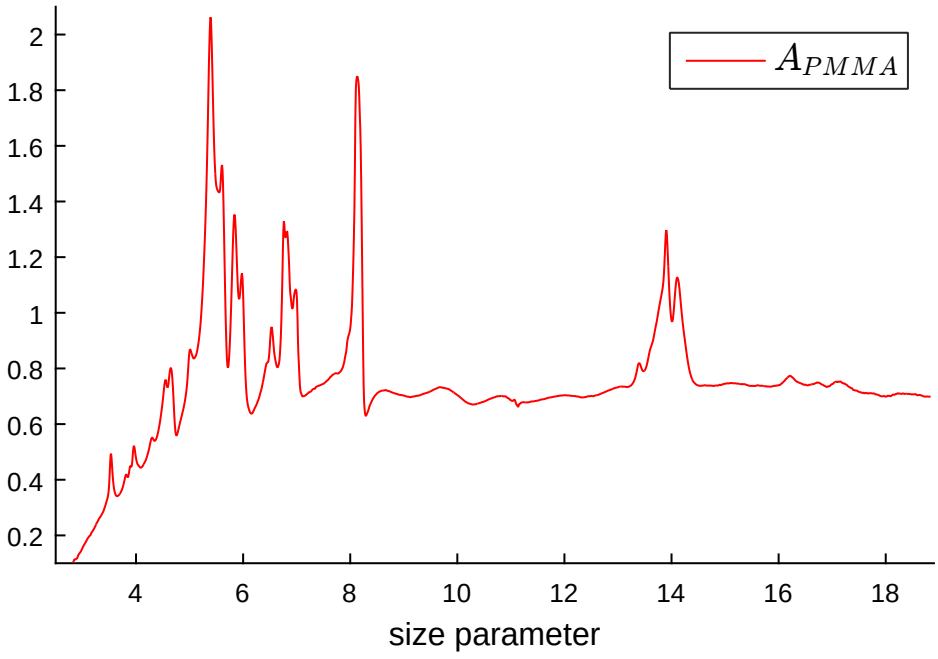

Figure 2.5: Example of an absorbance, A, from a PMMA sphere plotted with resolution $\Delta\tilde{\nu} = 4\text{cm}^{-1}$ and diameter 15μm.

2.2 Scattering of Light

This section is partly based on the book by Stone [13].

A beam of light which is incident on an object, i.e. a particle, as shown in figure 2.6, has power P_0 and intensity I_0. The object is placed between a light source and a detector with cross section G. The incident light is scattered, chemically absorbed by the object, and transmitted. The transmitted light has intensity I.

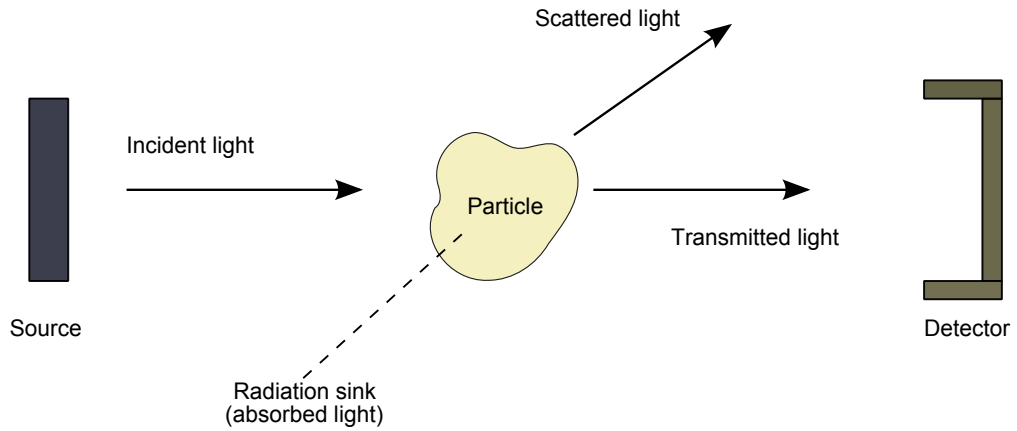

Figure 2.6: Illustration of scattered light. The incident light has intensity I_0. This light is scattered, chemically absorbed by the object, and part of the incident light is transmitted through to the detector. The transmitted light has intensity I.

The difference between the incident and the transmitted light is mainly because some of the light is scattered and some is absorbed by the particle. Thus scattering and absorption removes energy from the beam of light. This is called extinction and is defined as

$$Extinction = Scattering + Absorption$$

P_0 can be measured by removing the object from the path of the incident light. When an object is placed between the detector and the source, the detector measures a power P which is the power of the transmitted light. The incident light beam have lost power equivalent to $P_0 - P$ and is said to have experienced extinction. The lost power, P_{ext}, is distributed into two parts: P_{sca} and P_{abs}. P_{sca} is the power of a scattered wave radiated in various directions. The rest of the power is converted into heat generated in the interior of the object. This is called

absorption and has the power P_{abs}. Conservation of power requires that

$$P_0 = P + P_{sca} + P_{abs},$$

and the different powers are defined by the following equations

$$P_0 = GI_0, \qquad P = GI, \qquad P_{sca} = C_{sca}I_0, \qquad P_{abs} = C_{abs}I_0, \qquad P_{ext} = C_{ext}I_0,$$

where C_{ext}, C_{abs} and C_{sca} are the cross sections for extinction, scattering and absorption. Non-absorbing particles have $C_{ext} = C_{sca}$ and the law of conservation of energy requires that $C_{ext} = C_{sca} + C_{abs}$. I is the intensity of the transmitted light and I_0 the intensity of the incident light [13].

The extinction is often represented by Q_{ext} which is the extinction efficiency. The Q_{ext} describes the loss of of incident light, as a function of the wavelength, caused by the particle [5]

$$Q_{ext} = \frac{C_{ext}}{\text{cross- sectional area}}.$$

So for a sphere, with cross-sectional area $A = \pi a^2$, where a is the radius of the sphere, Q_{ext} is given by

$$Q_{ext} = \frac{C_{ext}}{\pi a^2}, \tag{2.1}$$

where C_{ext} is the extinction cross section and a is the radius of the sphere. The chemical quantity absorbance, A, is defined as

$$A = -log_{10}(T), \tag{2.2}$$

where T is the transmission. A conversion formula between Q_{ext} and A is given by

$$Q_{ext} = (1 - 10^{-A})\frac{G}{g},$$

where g is the geometrical cross section of the scatter and G is the area in front of the detector. Equation (2.2) can be rewritten as

$$A \approx \frac{\pi a^2}{Gln(10)}Q_{ext}, \tag{2.3}$$

where a is the radius of the sphere, G the area of the aperture in front of the detector. For convenience $\frac{\pi a^2}{G} \approx 0.05$ [10, 5].

2.2.1 Mie Theory

The extinction cross section, C_{ext}, is defined as

$$C_{ext} = \frac{2\pi}{k^2}\sum_{n=1}^{\infty}(2n+1)Re(\mathsf{a_n}+\mathsf{b_n}), \tag{2.4}$$

where k is the angular wavenumber given by $k = \frac{2\pi}{\lambda}$, λ is the wavelength in vacuum, and $\mathsf{a_n}$ and $\mathsf{b_n}$ are the scattering coefficients. The scattering coefficients, which are derived in appendix B, follows the notation used in Bohren, Huffman [5]. The connection between the extinction efficiency and the extinction cross section is defined by equation (2.1) which gives

$$Q_{ext} = \frac{2}{x^2}\sum_{n=1}^{\infty}(2n+1)Re(\mathsf{a_n}+\mathsf{b_n}), \tag{2.5}$$

where $x = ka$ is the size parameter. $\mathsf{a_n}$ is known as the electric mode and $\mathsf{b_n}$ the magnetic mode and they are given by the following

$$\left.\begin{aligned}\mathsf{a_n} &= \frac{m\psi_n(mx)\psi_n'(x)-\psi_n(x)\psi_n'(mx)}{m\psi_n(mx)\xi_n'(x)-\xi_n(x)\psi_n'(mx)}\\ \mathsf{b_n} &= \frac{\psi_n(mx)\psi_n'(x)-m\psi_n(x)\psi_n'(mx)}{\psi_n(mx)\xi_n'(x)-m\xi_n(x)\psi_n'(mx)}\end{aligned}\right\}, \tag{2.6}$$

where m is the refractive index, x is the size parameter, and ψ_n and ξ_n are the Riccati-Bessel functions which are defined by equation (B.0.4) in appendix B. As illustrated in this section, for calculations using Mie theory, it is necessary to know the radius of the scattering particle, a, and the refractive index, m which can be complex.

The complex refractive index, m, consists of a real and a imaginary part, respectively $\tilde{n}$ and $\tilde{n}'$. The relation between these terms are given by

$$m(\tilde{\nu}) = \tilde{n}(\tilde{\nu}) + i\tilde{n}'(\tilde{\nu}), \tag{2.7}$$

following the notation in [16]. In equation (2.7) $\tilde{\nu}$ is the wavenumber, $\tilde{n}$ describes the refractive properties of the material and $\tilde{n}'$ describes the absorptive properties of the material.

2.3 Ripple Structure

The extinction efficiency, Q_{ext}, is given by equation (2.5) and is a function of the size parameter. In figure 2.7 the extinction efficiency is plotted from $x = 0$ to

$x = 30$. As x increases the peaks in the ripple structure becomes sharper. These ripples are also called resonances and are, as illustrated in figure 2.7, superimposed on top of large oscillations in the baseline. This structure is also present in the absorbance, A, given by equation (2.3) and illustrated in figure 2.8.

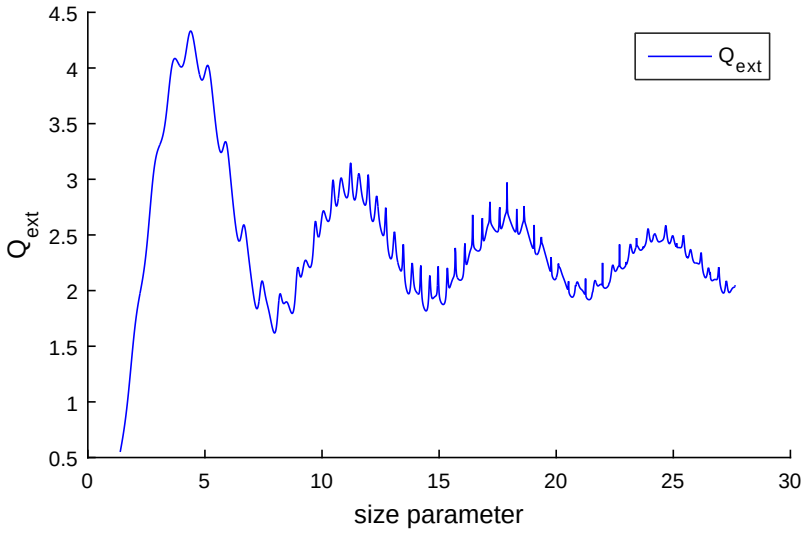

Figure 2.7: Extinction efficiency Q_{ext} as a function of size parameter x.

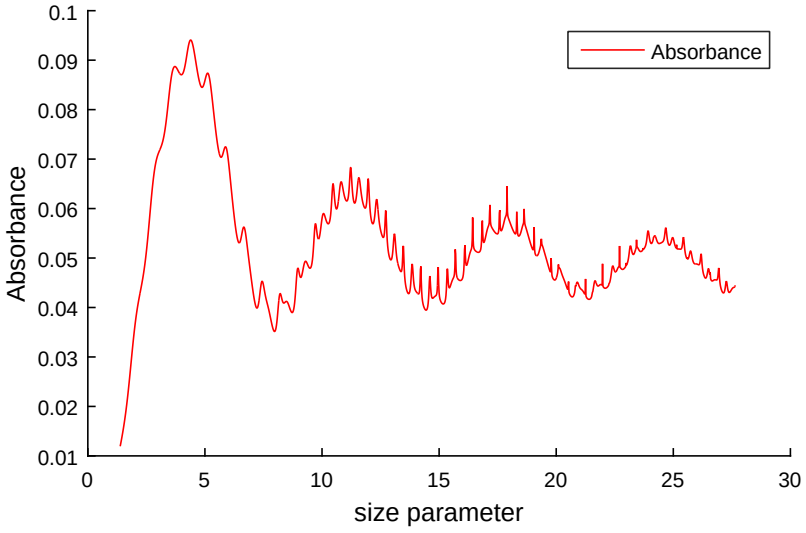

Figure 2.8: Absorbance A as a function of size parameter x.

2.3.1 Approximation Formula for Distances Between Resonances

The distinct ripple structure in the extinction efficiency, Q_{ext}, as illustrated in figure 2.7, is caused by the summation of the real parts of a_n and b_n, given by equation (2.6). In figure 2.9 the $\sum \mathsf{a}_n$ and the $\sum \mathsf{b}_n$ are plotted in the same figure.

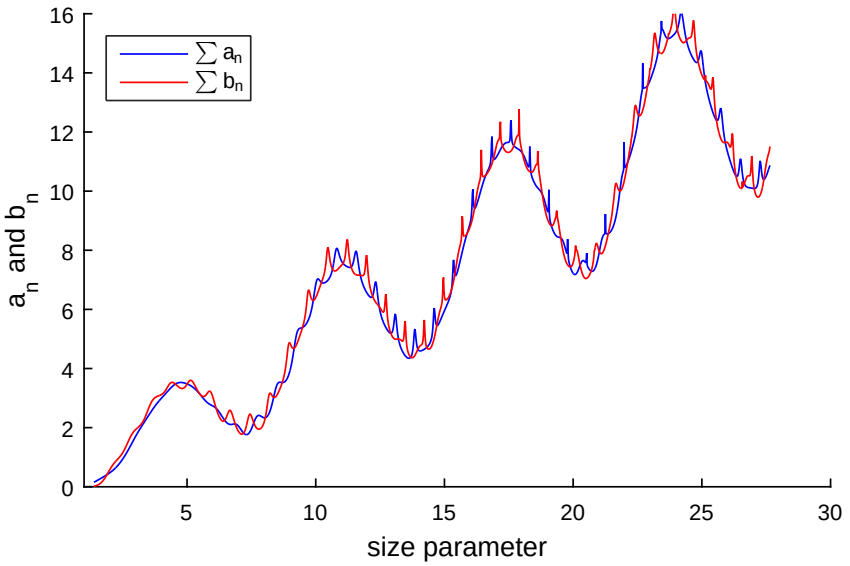

Figure 2.9: $\sum \mathsf{a}_n$ and $\sum \mathsf{b}_n$ as a function of size parameter.

The peaks in $\sum \mathsf{a}_n$ and $\sum \mathsf{b}_n$ are also called resonances and their notation are shown in figure 2.10. The first peak of the electric mode a with index $n = 20$ would be denoted as $\mathsf{a}_{20}{}^{1}$.

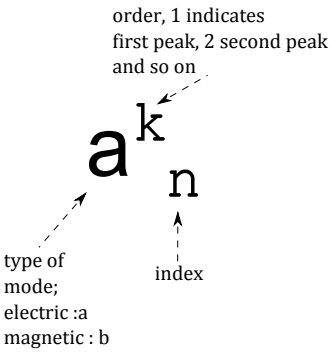

Figure 2.10: Illustration of the notation of $\mathsf{a}_n{}^{k}$ where k is the order of the resonance, n is the index or the number of the resonance.

The distance between the resonances is represented by dx. The position of these distances are illustrated in figure 2.11.

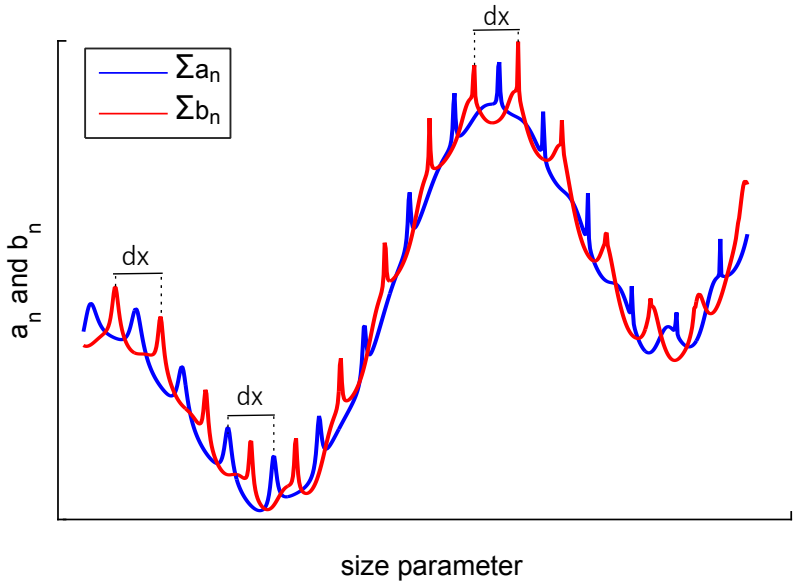

Figure 2.11: $\sum \mathsf{a_n}$ and $\sum \mathsf{b_n}$ as a function of size parameter. dx is the distance between the resonances.

In 1975, Petr Chỳlek [6] derived a formula for this distance between the resonances, the sharp peaks in Q_{ext}, the extinction efficiency. This formula is only dependent on the refractive index m of the sphere and is defined as

$$dx = \frac{tan^{-1}\sqrt{m^2-1}}{\sqrt{m^2-1}}. \tag{2.8}$$

Equation (2.8) was further developed by Petr Chỳlek, and in 1990 [7], a new and improved approximation formula for dx was derived

$$dx = \frac{x \cdot tan^{-1}((\frac{mx}{n})^2-1)^{1/2}}{n((\frac{mx}{n})^2-1)^{1/2}}, \tag{2.9}$$

where x is the position of the peak, n the index of the peak and m the refractive index. The distance dx calculated by equation (2.9) is the distance between two successive resonances of the same order k. So, the size parameter distance, $dx_n^{(k)}$, between $\mathsf{a_n}^{(k)}$ and $\mathsf{a_{n+1}}^{(k)}$ is given by $dx_n^{(k)} = x_{n+1}^{(k)} - x_n^{(k)}$. Equation (2.8) and equation (2.9) are defined to hold under the assumptions $x \gg 1$, $n \gg 1$, $\frac{x}{n} \sim 1$ and $mx \sim n$. The assumption that $\frac{x}{n} \sim 1$ indicates that $\mathsf{a_{20}}$ will have its first peak, $\mathsf{a_{20}}^1$, in close proximity of $x = 20$.

Chapter 3

Results

3.1 Effect on Ripple Structure by Changing Resolution

The resolution is here referred to as the step size in the wavenumber or the size parameter. A low resolution results in a fine grid. It is given as a step in the wavenumber, $\Delta\tilde{\nu}$, and can be converted to size parameter, Δx, by

$$\Delta x = 2\pi \times \Delta\tilde{\nu} \times 100 \times a, \qquad \Delta\tilde{\nu} = \frac{\Delta x}{2\pi \times 100 \times a}, \tag{3.1}$$

where a is the radius of the sphere. In the following figures the functions are given as functions of the size parameter x as frequently done in the literature. The resolution is on the other hand given as a step in the wavenumber $\tilde{\nu}$ for convenience. This conversion formula, equation 3.1, is therefore useful. For example, $\Delta\tilde{\nu} = 10\text{cm}^{-1}$ corresponds to a resolution of $\Delta x \approx 0.035$, $\Delta\tilde{\nu} = 5\text{cm}^{-1}$ corresponds to $\Delta x \approx 0.017$, and $\Delta\tilde{\nu} = 0.2\text{cm}^{-1}$ corresponds to $\Delta x \approx 0.00069$.

In this thesis, a refractive index of $m = 1.48$ and a radius of $a = 5.5 \times 10^{-6}\text{m}$, is the main area of study. The reason for choosing this refractive index is because the real part of the refractive index for PMMA are approximately $m = 1.48$ [10]. For the radius of the sphere, it is assumed to lie in the interval $[1\mu\text{m}; 10\mu\text{m}]$ [10].

Figure 3.1 shows the extinction efficiency Q_{ext} as a function of size parameter x with a refractive index $m = 1.48$ and a radius of the sphere $a = 5.5 \times 10^{-6}\text{m}$ on the interval $0 < x < 28$. Q_{ext} is plotted with $\Delta\tilde{\nu} = 5\text{cm}^{-1}$ and oscillate around 2.5. The ripple structure is superimposed on large oscillations and it becomes more prominent as x increases. Figure 3.1 is generated using the Matlab script *PlotQext.m* [14].

In figure 3.2 the resolution is changed from $\Delta\tilde{\nu} = 5\text{cm}^{-1}$ to $\Delta\tilde{\nu} = 0.2\text{cm}^{-1}$.

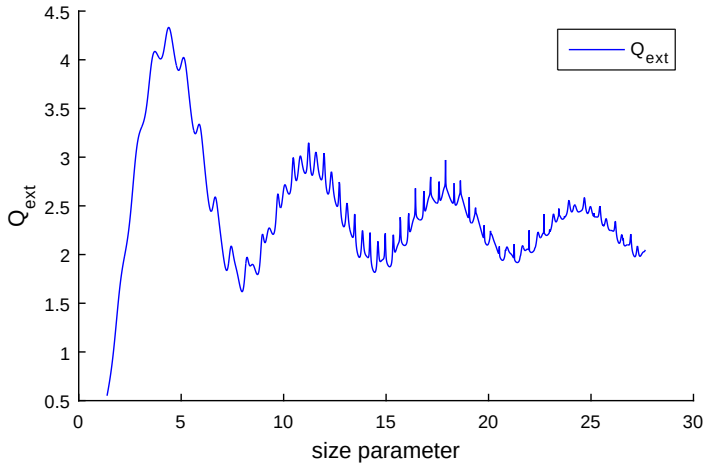

Figure 3.1: Extinction efficiency Q_{ext} as a function of size parameter x employing a resolution of $\Delta\tilde{\nu} = 5\text{cm}^{-1}$, a refractive index of $m = 1.48$ and a radius of the sphere of $a = 5.5 \times 10^{-6}\text{m}$ on the interval $1 < x < 28$. On top of the large oscillations a ripple structure is observed, which becomes more pronounced as x is increased.

One clear change from figure 3.1 is that the height of the sharp peaks have increased from $x \approx 17$.

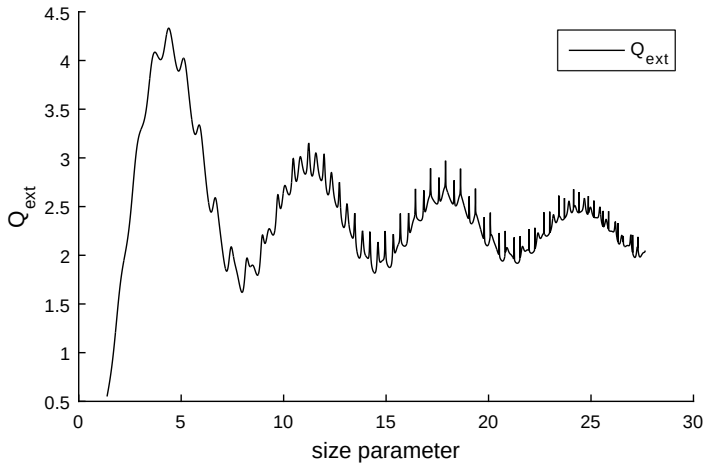

Figure 3.2: Extinction efficiency Q_{ext} as a function of size parameter x employing a resolution of $\Delta\tilde{\nu} = 0.2\text{cm}^{-1}$, a refractive index of $m = 1.48$ and a radius of the sphere of $a = 5.5 \times 10^{-6}\text{m}$ on the interval $1 < x < 28$. On top of the large oscillations a ripple structure is observed, which becomes more pronounced as x is increased.

As illustrated by figure 3.1 and figure 3.2 a change in the resolution gives a

visual change in the spectra of Q_{ext}. In figure 3.3 $\sum \mathsf{a_n}$, $\sum \mathsf{b_n}$ and Q_{ext} are plotted together as functions of size parameter x on the interval $1 < x < 28$ for refractive index $m = 1.48$ and radius of the sphere $a = 5.5 \times 10^{-6}$m. From $x \approx 10$ a distinct ripple structure is visible and by observation it is clear that every second peak is $\mathsf{a_n}$ and $\mathsf{b_n}$. As in Q_{ext}, illustrated by figure 3.1 and figure 3.2, the ripple structure becomes sharper as x is increased. This figure is generated using the Matlab script *Plot_An_Bn_oneplot.m* [14].

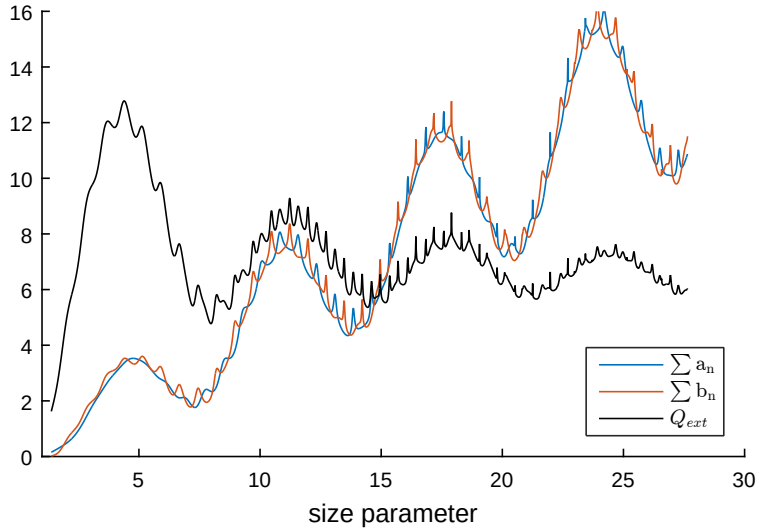

Figure 3.3: $\sum \mathsf{a_n}$, $\sum \mathsf{b_n}$ and Q_{ext} as a function of size parameter employing a resolution of $\Delta\tilde{\nu} = 5\text{cm}^{-1}$, a refractive index of $m = 1.48$ and a radius of the sphere of $a = 5.5 \times 10^{-6}$m on the interval $1 < x < 28$.

3.1.1 Effect of the Resolution on $\mathsf{a_n}$ and $\sum \mathsf{a_n}$

As stated in chapter 2.3.1, when calculating dx, the distance between the peaks in the resonance structure, according to equation (2.9), the distance has to be taken between successive peaks of the same order and of the same mode, electric or magnetic. It is therefore interesting to investigate how a change of the resolution in $\sum \mathsf{a_n}$ affects the ripple structure. Each single $\mathsf{a_n}$ contributes to the ripple structure in $\sum \mathsf{a_n}$, as shown in figure 3.3. Thus, it is important to know, if the resolution changes appearance of certain peaks in $\sum \mathsf{a_n}$. Further, it is of interest to determine if the visible peaks are first, second or third order peaks.

Figure 3.4 shows $\sum \mathsf{a_n}$ as a function of the size parameter x, using a refractive index of $m = 1.48$ and a radius of the sphere of $a = 5.5 \times 10^{-6}$m. Figure 3.4a is plotted with resolution $\Delta\tilde{\nu} = 0.2\text{cm}^{-1}$ and figure 3.4b is plotted with

$\Delta\tilde{\nu} = 10\text{cm}^{-1}$. From $x \approx 20$ a clear change is visible when the resolution is decreased. In figure 3.4a high, sharp peaks as well as wide peaks are visible, while in figure 3.4b this area contains wider peaks.

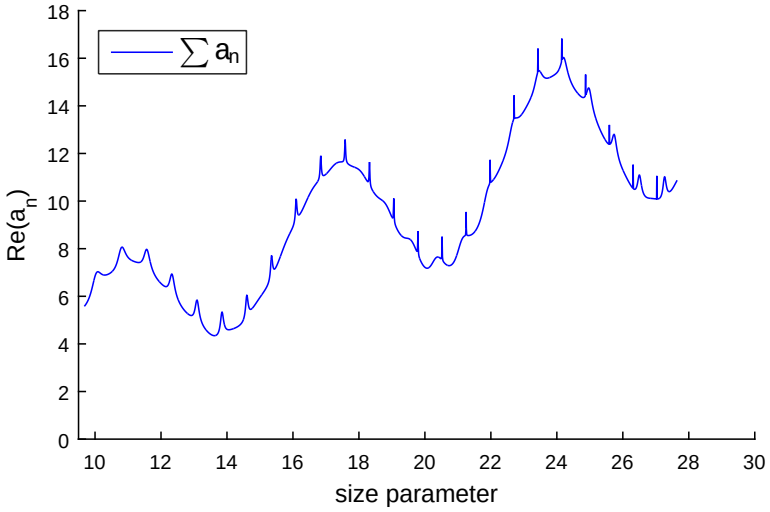

(a)

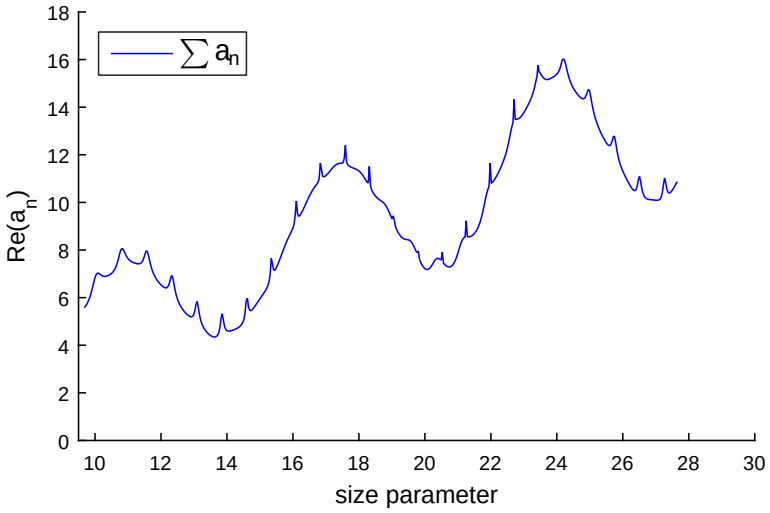

(b)

Figure 3.4: $\sum a_n$ with a refractive index of $m = 1.48$ and a radius of the sphere of $a = 5.5 \times 10^{-6}\text{m}$. (**a**) Resolution $\Delta\tilde{\nu} = 0.2\text{cm}^{-1}$. (**b**) Resolution $\Delta\tilde{\nu} = 10\text{cm}^{-1}$.

As figure 3.4 shows, the ripple structure change when the resolution change. For higher values of the size parameter, high resolution results in higher and

shaper peaks in the ripple structure. In figure 3.5 the area that changes most in figure 3.4 is zoomed in on. The same refractive index and radius as in figure 3.4 is applied. In figure 3.5a the resolution is $\Delta\tilde{\nu} = 0.2\text{cm}^{-1}$, in figure 3.5b $\Delta\tilde{\nu} = 0.9\text{cm}^{-1}$, in figure 3.5c $\Delta\tilde{\nu} = 5\text{cm}^{-1}$ and in figure 3.5d $\Delta\tilde{\nu} = 10\text{cm}^{-1}$.

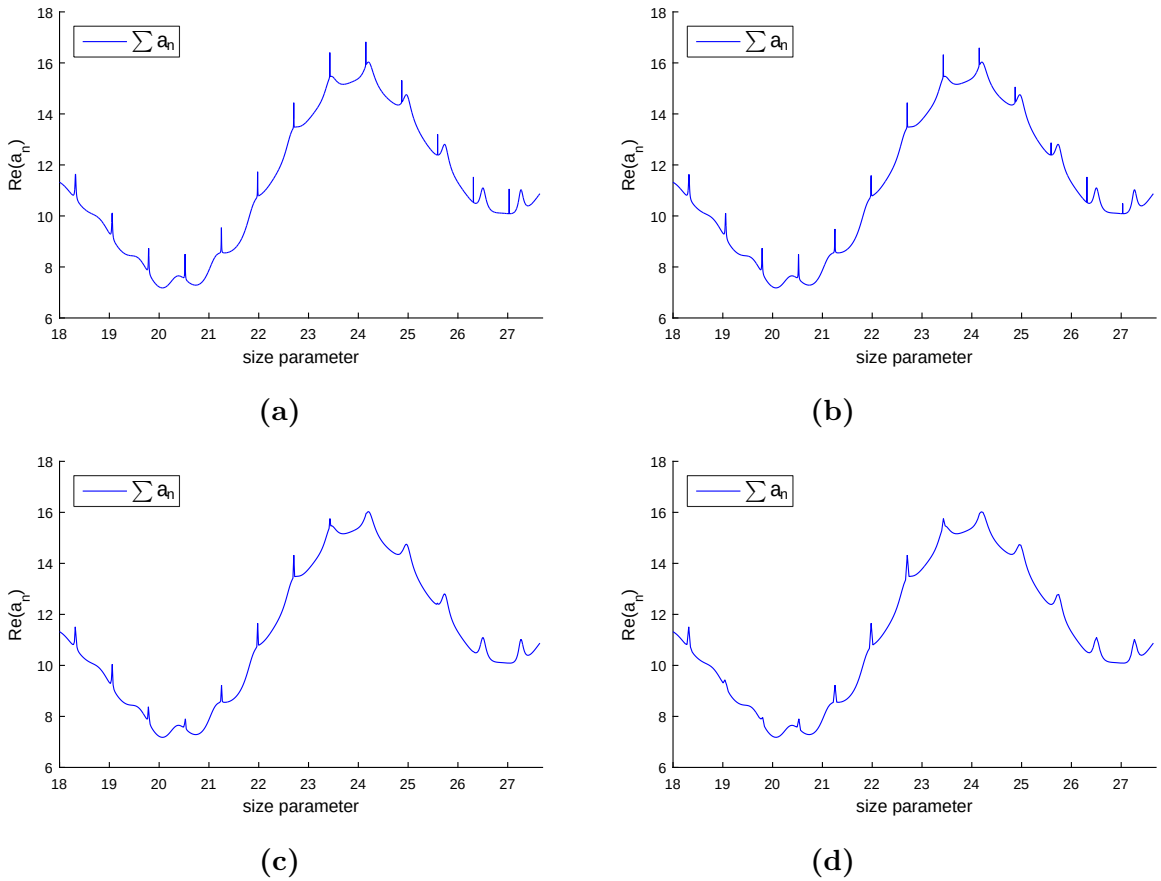

Figure 3.5: Plot of $\sum \mathsf{a_n}$ with a refractive index of $m = 1.48$, a radius of the sphere of $a = 5.5 \times 10^{-6}$m and decreasing resolution. (**a**) Resolution $\Delta\tilde{\nu} = 0.2\text{cm}^{-1}$. (**b**) Resolution $\Delta\tilde{\nu} = 0.9\text{cm}^{-1}$. (**c**) Resolution $\Delta\tilde{\nu} = 5\text{cm}^{-1}$. (**d**) Resolution $\Delta\tilde{\nu} = 10\text{cm}^{-1}$.

It is not likely to get spectra from biological material with resolution as high resolution as $\Delta\tilde{\nu} = 0.2\text{cm}^{-1}$. Lukacs et al.[10] recorded samples with $\Delta\tilde{\nu} = 4\text{cm}^{-1}$ for PMMA spheres. So, it might therefore be a good idea to work with resolution $\Delta\tilde{\nu} = 5\text{cm}^{-1}$ as in figure 3.5c where the peaks in the area $19 < x < 20$ still are clear and visible.

In figure 3.6 the $\mathsf{a_n}$ is plotted together with $\mathsf{a_{26}}$, $\mathsf{a_{30}}$ and $\mathsf{a_{34}}$ as a function of the size parameter x. The resolution is $\Delta\tilde{\nu} = 10\text{cm}^{-1}$, the refractive index $m = 1.48$ and the radius of the sphere $a = 5.5 \times 10^{-6}$m. As stated in chapter 2.3.1, the

ripple structure in $\sum \mathsf{a_n}$ is due to the sum of the single $\mathsf{a_n}$. When plotting with $\Delta\tilde{\nu} = 10\text{cm}^{-1}$ it appears that the peak around $x = 24$ is caused by the secondary peak of $\mathsf{a_{26}}$ and not by the first peak of $\mathsf{a_{30}}$ which is small and not very prominent. Figure 3.6 is generated using the Matlab script *Plot_many_single_an.m* [14].

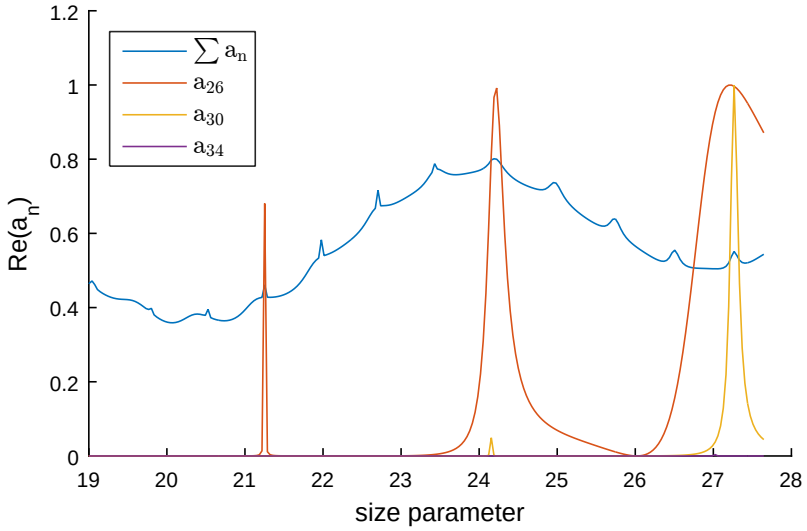

Figure 3.6: $\sum \mathsf{a_n}$ and $\mathsf{a_{26}}$, $\mathsf{a_{30}}$ and $\mathsf{a_{34}}$ as a function of the size parameter x employing a resolution of $\Delta\tilde{\nu} = 10\text{cm}^{-1}$, a refractive index of $m = 1.48$ and a radius of the sphere of $a = 5.5 \times 10^{-6}\text{m}$.

When the resolution is high, i.e. $\Delta\tilde{\nu} = 0.2\text{cm}^{-1}$, the $\sum \mathsf{a_n}$ has a ripple structure consisting of alternating sharp and wide peaks. This is illustrated in figure 3.5a. In figure 3.7 $\sum \mathsf{a_n}$ is plotted together with $\mathsf{a_{26}}$, $\mathsf{a_{30}}$ and $\mathsf{a_{34}}$ as a function of the size parameter x. Figure 3.7 is employed with a resolution of $\Delta\tilde{\nu} = 0.2\text{cm}^{-1}$, a refractive index of $m = 1.48$ and a radius of the sphere of $a = 5.5 \times 10^{-6}\text{m}$. When plotting with $\Delta\tilde{\nu} = 0.2\text{cm}^{-1}$, the first order peaks of $\mathsf{a_{26}}$, $\mathsf{a_{30}}$ and $\mathsf{a_{34}}$ are prominent and the position of these peaks coincide with the high and sharp peaks in $\sum \mathsf{a_n}$. The second order peaks of $\mathsf{a_{26}}$ and $\mathsf{a_{30}}$ coincide with the wider peaks in $\sum \mathsf{a_n}$. Thus, when the resolution is high, the first order peaks are responsible for the sharp peaks and the second order peaks are responsible for the wider peaks in $\sum \mathsf{a_n}$.

When $\sum \mathsf{a_n}$ is plotted together with $\mathsf{a_{26}}$, $\mathsf{a_{30}}$ and $\mathsf{a_{34}}$ with resolution $\Delta\tilde{\nu} = 10\text{cm}^{-1}$ (see figure 3.6), it appears that the peak in $\sum \mathsf{a_n}$ around $x = 27.5$ is caused by the second order peak of $\mathsf{a_{30}}$ and not by the first order peak of $\mathsf{a_{34}}$. The same is evident for the peak around $x = 24$ which appears to be caused by the second order peak of $\mathsf{a_{26}}$ and not by the first order peak of $\mathsf{a_{30}}$. In contrast, the first order peak for $\mathsf{a_{34}}$ and the sharp ripple in $\sum \mathsf{a_n}$ (behind the first peak of

a_{34}) in figure 3.7 coincide perfectly. The second order peak of a_{30} and the wider peak coincide perfectly.

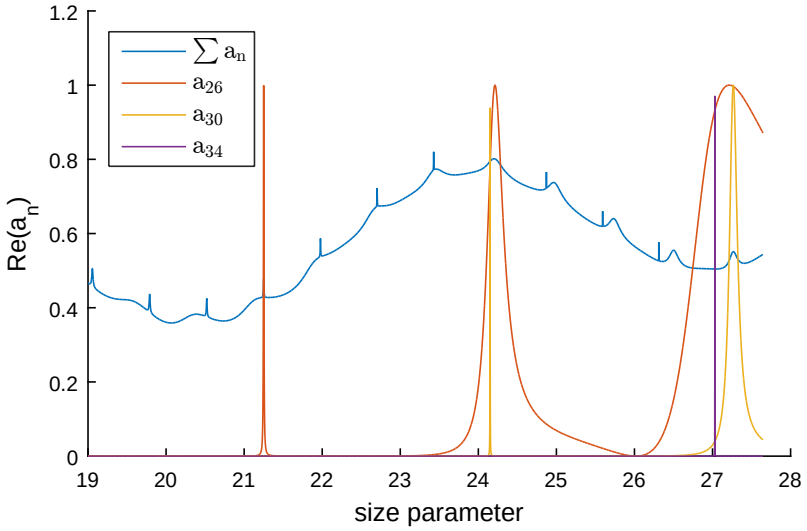

Figure 3.7: $\sum a_n$ and a_{26}, a_{30} and a_{34} as a function of the size parameter x employing a resolution $\Delta\tilde{\nu} = 0.2\text{cm}^{-1}$, a refractive index $m = 1.48$ and radius of the sphere of $a = 5.5 \times 10^{-6}\text{m}$.

In figure 3.8, sharp peaks in addition to the wider peaks in the upper part of the size parameter. Just by changing the resolution from $\Delta\tilde{\nu} = 0.2\text{cm}^{-1}$ to $\Delta\tilde{\nu} = 2\text{cm}^{-1}$ in figure 3.8, the height of the sharp peaks are reduced.

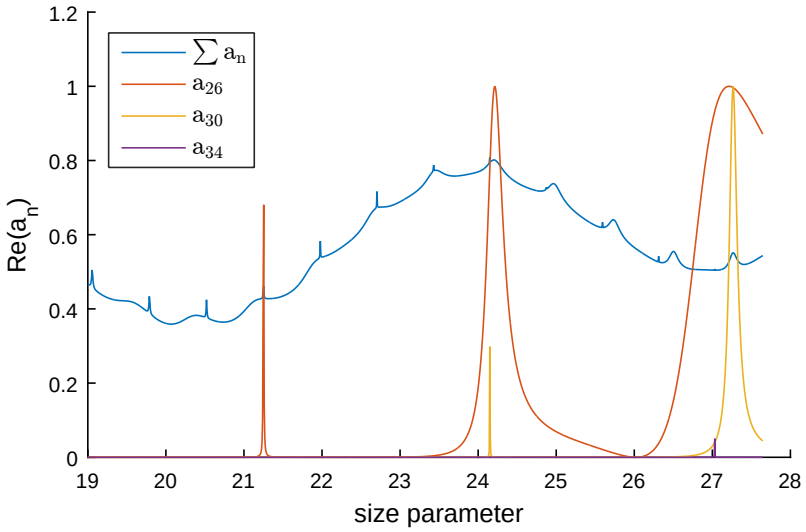

Figure 3.8: $\sum \mathsf{a_n}$ and $\mathsf{a_{26}}$, $\mathsf{a_{30}}$ and $\mathsf{a_{34}}$ as a function of the size parameter x employing a resolution $\Delta\tilde{\nu} = 2\text{cm}^{-1}$, a refractive index $m = 1.48$ and a radius of the sphere of $a = 5.5 \times 10^{-6}\text{m}$.

As figure 3.9a and 3.9b illustrates, the height of the first peaks of $\mathsf{a_{30}}$ and $\mathsf{a_{34}}$ is reduced when decreasing the resolution from $\Delta\tilde{\nu} = 5\text{cm}^{-1}$ in (**a**) to $\Delta\tilde{\nu} = 10\text{cm}^{-1}$ in (**b**). Low resolution, as illustrated in figure 3.9b, creates wider peaks in $\sum \mathsf{a_n}$.

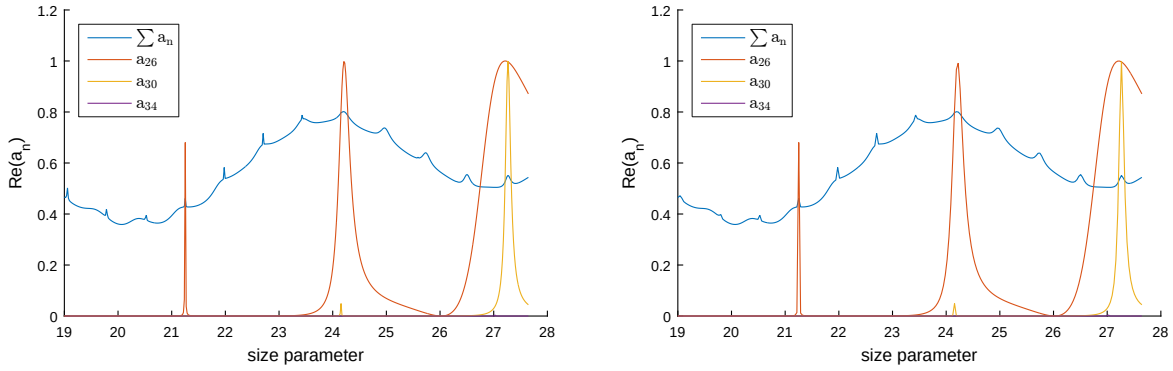

Figure 3.9: $\sum \mathsf{a_n}$ and $\mathsf{a_{26}}$, $\mathsf{a_{30}}$ and $\mathsf{a_{34}}$ as a function of the size parameter x employing a refractive index $m = 1.48$ and a radius of the sphere of $a = 5.5 \times 10^{-6}\text{m}$. (**a**) $\Delta\tilde{\nu} = 5\text{cm}^{-1}$. (**b**) $\Delta\tilde{\nu} = 10\text{cm}^{-1}$.

Next, single $\mathsf{a_n}$ is plotted together with $\sum \mathsf{a_n}$ in several plots. Instead of plotting all single $\mathsf{a_n}$ together with the sum in one plot, the range $0 < x < 28$ is distributed to six different graphs. For convenience the size parameter range used in the different plots overlap. The reason for this overlap is to make the graphs easier to read and understand. Further, some of the $\mathsf{a_n}$ are repeated in the different plots to facilitate comparison. The index n range from 8 to 34 in figure 3.11 to figure 3.15. In these figures (3.11 to 3.15), both the subplots in each figure are plotted over the same range of size parameter and with the same $\mathsf{a_n}$. A refractive index of $m = 1.48$ and a radius of the sphere of $a = 5.5 \times 10^{-6}$m was chosen. Each subplot contains one figure plotted with $\Delta\tilde{\nu} = 0.2\text{cm}^{-1}$ on the left side and $\Delta\tilde{\nu} = 2\text{cm}^{-1}$ on the right side. In figure 3.10 $\mathsf{a_8}$ to $\mathsf{a_{13}}$ are plotted, in figure 3.11 $\mathsf{a_{13}}$ to $\mathsf{a_{18}}$, in figure 3.12 $\mathsf{a_{18}}$ to $\mathsf{a_{23}}$, in figure 3.13 $\mathsf{a_{23}}$ to $\mathsf{a_{27}}$, in figure 3.14 $\mathsf{a_{27}}$ to $\mathsf{a_{31}}$ and in figure 3.15 $\mathsf{a_{30}}$ to $\mathsf{a_{34}}$.

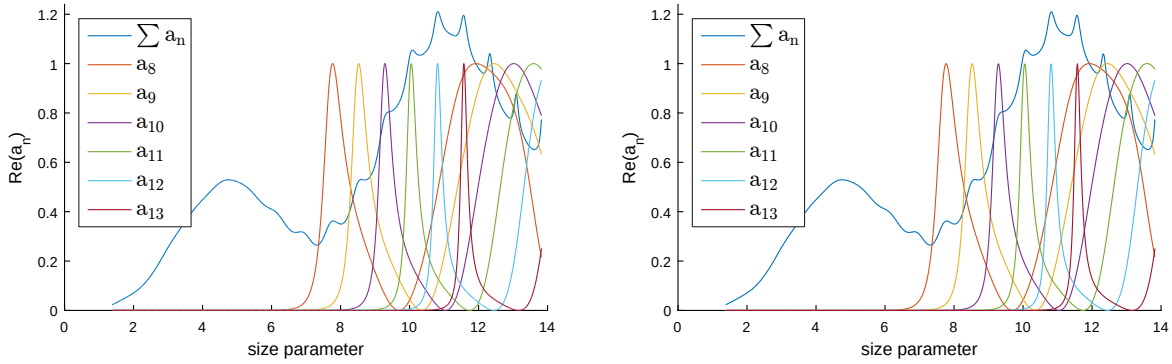

Figure 3.10: Plot of $\sum \mathsf{a_n}$ and $\mathsf{a_n}$ with index ranging from $n = 8$ to $n = 13$. (**a**) Resolution $\Delta\tilde{\nu} = 0.2\text{cm}^{-1}$. (**b**) Resolution $\Delta\tilde{\nu} = 5\text{cm}^{-1}$.

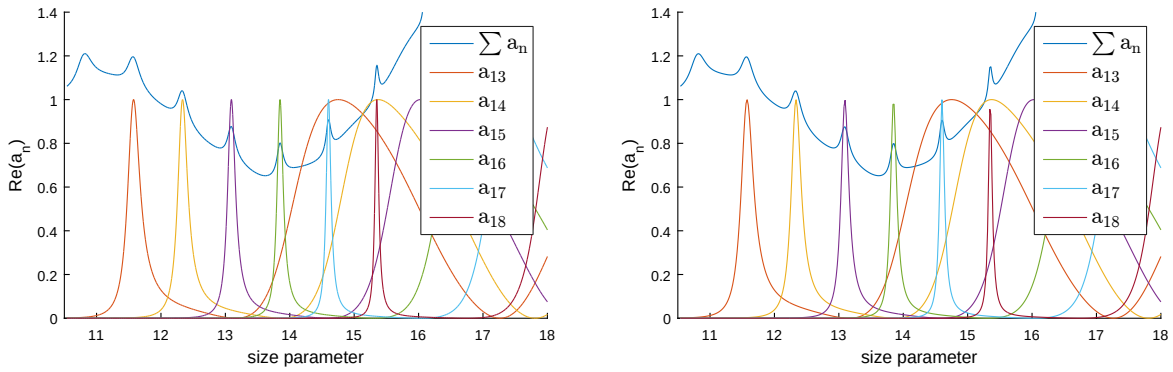

(a) **(b)**

Figure 3.11: Plot of $\sum \mathsf{a_n}$ and $\mathsf{a_n}$ with index ranging from $n = 13$ to $n = 18$. (**a**) Resolution $\Delta\tilde{\nu} = 0.2\text{cm}^{-1}$. (**b**) Resolution $\Delta\tilde{\nu} = 5\text{cm}^{-1}$.

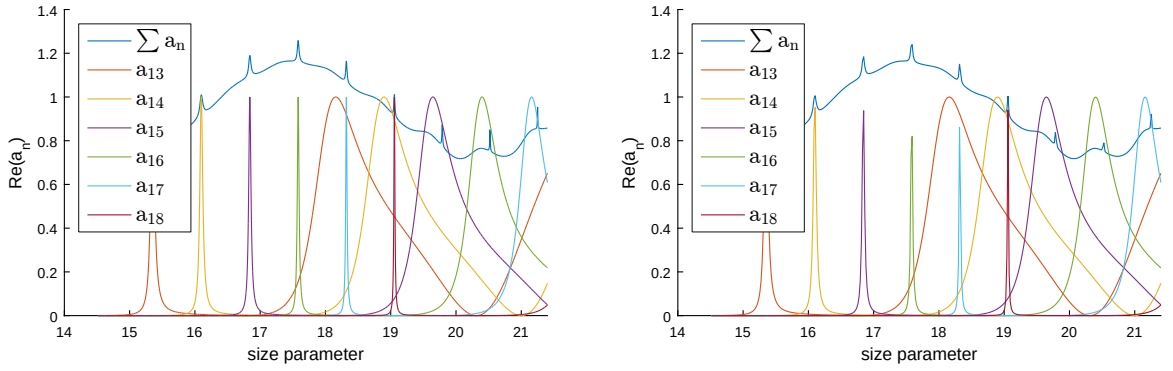

(a) **(b)**

Figure 3.12: Plot of $\sum \mathsf{a_n}$ and $\mathsf{a_n}$ with index ranging from $n = 18$ to $n = 23$. (**a**) Resolution $\Delta\tilde{\nu} = 0.2\text{cm}^{-1}$. (**b**) Resolution $\Delta\tilde{\nu} = 5\text{cm}^{-1}$.

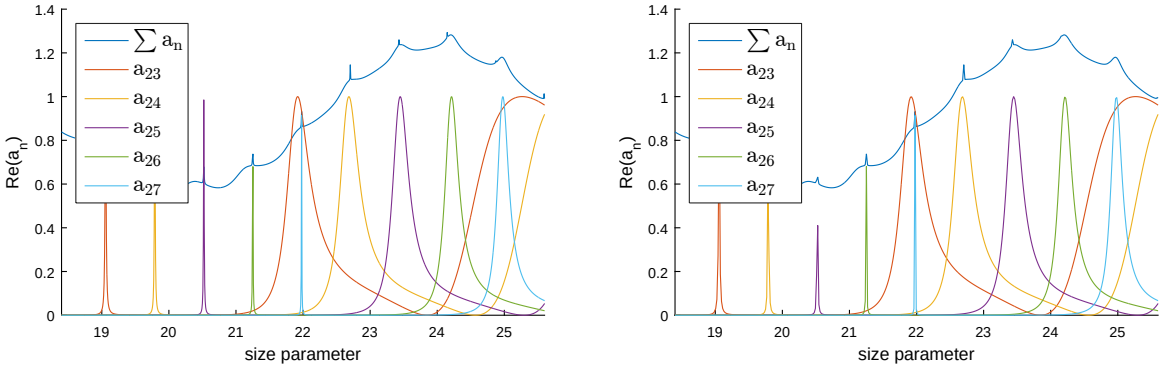

(a) **(b)**

Figure 3.13: Plot of $\sum \mathsf{a_n}$ and $\mathsf{a_n}$ with index ranging from $n = 23$ to $n = 27$. (**a**) Resolution $\Delta\tilde{\nu} = 0.2\text{cm}^{-1}$. (**b**) Resolution $\Delta\tilde{\nu} = 5\text{cm}^{-1}$.

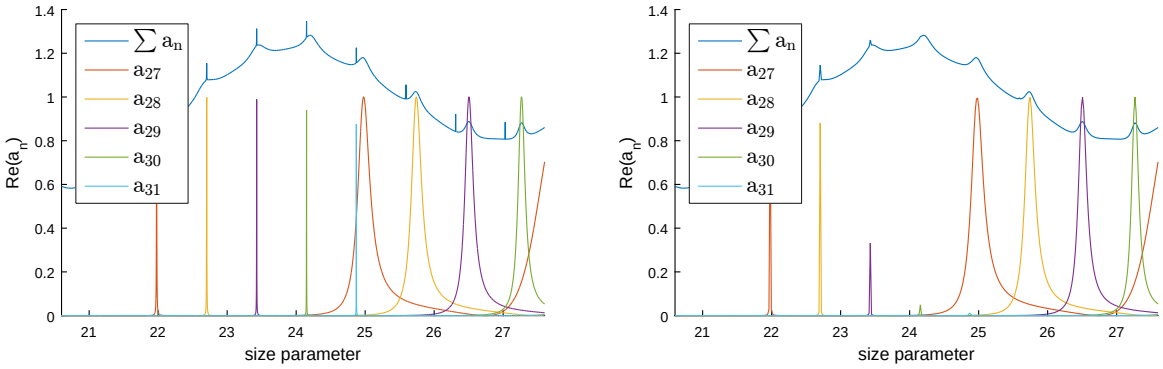

(a) **(b)**

Figure 3.14: Plot of $\sum \mathsf{a_n}$ and $\mathsf{a_n}$ with index ranging from $n = 27$ to $n = 31$. (**a**) Resolution $\Delta\tilde{\nu} = 0.2\text{cm}^{-1}$. (**b**) Resolution $\Delta\tilde{\nu} = 5\text{cm}^{-1}$.

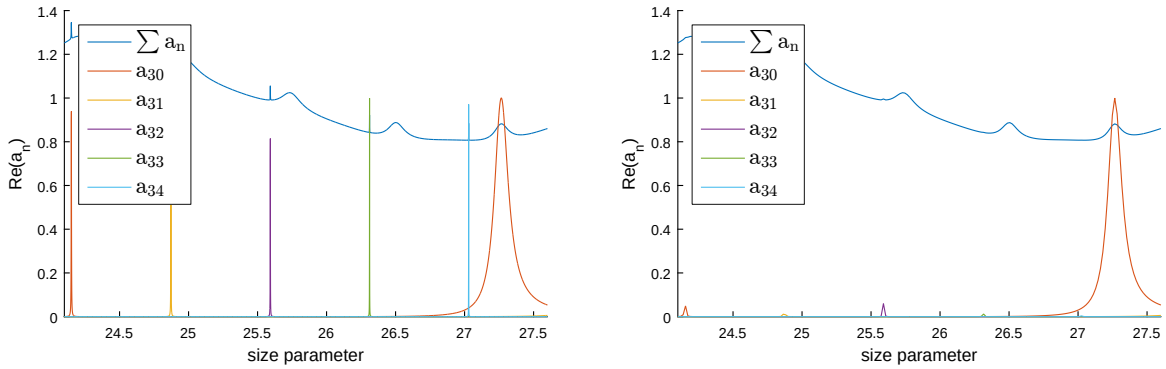

(a) **(b)**

Figure 3.15: Plot of $\sum \mathsf{a_n}$ and $\mathsf{a_n}$ with index ranging from $n = 30$ to $n = 34$. (**a**) Resolution $\Delta\tilde{\nu} = 0.2\text{cm}^{-1}$. (**b**) Resolution $\Delta\tilde{\nu} = 5\text{cm}^{-1}$.

In figure 3.10 and figure 3.11 the second order peaks only contribute to the background oscillation in the baseline while the first order peaks create the ripple structure. In figure 3.13a, figure 3.14a and figure 3.15a the secondary peaks creates a wide peak after a sharp peak. The effect of the change in the resolution is first evident in figure 3.13. The first order peaks in figure 3.13b are not as prominent as in 3.13a. When comparing 3.15a and 3.15b it becomes clear that for low resolution, i.e. $\Delta\tilde{\nu} = 5\text{cm}^{-1}$, the second order peaks are responsible for the ripple structure in the higher range of the size parameter.

3.2 Approximation Formulas for the Distance Between the Resonances

It is of general interest to see how accurate the approximation formulas, given in chapter 2.3.1, for the distance between the peaks in the $\sum \mathsf{a_n}$ and $\sum \mathsf{b_n}$ are, and if these formulas can be used for other purposes. One important area of application can be to use these formulas for the calculation of the refractive index from $\sum \mathsf{a_n}$.

3.2.1 Accuracy of Approximation Formulas for Calculating dx

In this section, the accuracy of the equations for calculating dx, given in chapter 2.3.1, is investigated. The results from equation (2.8) and equation (2.9) are compared to the results from the actual distances obtained numerically from the exact Mie solutions. Finally these results are compared with the distances between the

peak positions of single $\mathsf{a_n}$. Throughout this section *Exact* is the distance between the peaks in $\sum \mathsf{a_n}$. *Exact single* $\mathsf{a_n}$ is is the distance, dx, between the first order peaks for each $\mathsf{a_n}$. *Complicated formula* is the distance, dx, calculated using equation (2.9), which takes the position and the index of the resonances into account. *Simple formula* is the distance between the peaks calculated using equation (2.8).

In figure 3.16 the results from calculating the distance between the peaks, dx, using equation (2.9) (*Complicated formula*), equation (2.8) (*Simple formula*) and with the dx obtained numerically from the exact Mie solution (*Exact*) are compared. *Exact* is calculated from the peaks in $\sum \mathsf{a_n}$ where a radius of the sphere of $a = 5.5 \times 10^{-6}$m, a refractive index of $m = 1.48$ and a resolution of $\Delta\tilde{\nu} = 5\text{cm}^{-1}$ was employed. This result is computed for $n = 12$ to $n = 57$ because the first peaks for $n < 12$ in $\sum \mathsf{a_n}$ is not very prominent. The results are generated using the Matlab script *Simulation3.m* [14]. Figure 3.16 illustrates the results, and the numerical results can be found in table C.1 in appendix C.

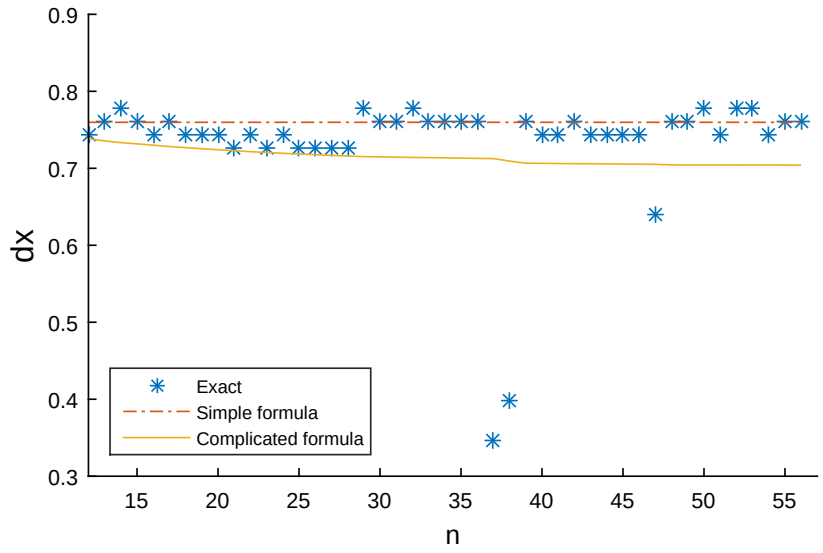

Figure 3.16: *Exact* is the dx calculated from the peaks of $\sum \mathsf{a_n}$ with a radius of the sphere of $a = 5.5 \times 10^{-6}$m (blue), a refractive index $m = 1.48$ and a resolution of $\Delta\tilde{\nu} = 5\text{cm}^{-1}$, *Complicated formula* is the dx calculated using equation (2.9) (yellow) and *Simple formula* is the dx calculated using equation (2.8) (orange). The numerical values are given in table C.1 in appendix C.

In figure 3.16 the distance dx between adjacent peaks of $\sum \mathsf{a_n}$ is displayed. From this figure it appears as equation (2.9) (*Complicated formula*) for calculating dx might be the best approximation from $n = 12$ to $n \approx 30$. The distances

from $n = 30$ until $n = 57$ are approximated better with equation (2.8) (*Simple formula*).

In figure 3.17 the results from calculating the distance between the peaks, dx, using equation (2.9) (*Complicated formula*), equation (2.8) (*Simple formula*), with the dx obtained numerically from the exact Mie solution (*Exact*) and with the distance, dx, between the first order peaks for each $\mathsf{a_n}$ (*Exact single* $\mathsf{a_n}$) are compared. For all calculations a radius of the sphere of $a = 5.5 \times 10^{-6}$m, a refractive index $m = 1.48$ and a resolution of $\Delta\tilde{\nu} = 5\text{cm}^{-1}$ was used. The positions of the first peaks for the single $\mathsf{a_n}$ are computed with resolution $\Delta x = 0.0173$ which is equivalent to $\Delta\tilde{\nu} = 5\text{cm}^{-1}$ calculated with equation (3.1). These results are computed for $n = 12$ to $n = 57$ because the prominence of the first peaks for $n < 12$ in $\sum \mathsf{a_n}$ are not distinct and it would be difficult to separate one peak from the other. The results are generated using the Matlab script *Plot_different_deltax_results_n12_57.m* [14]. The results are illustrated in figure 3.17 and the numerical results are given in table C.2 in appendix C.

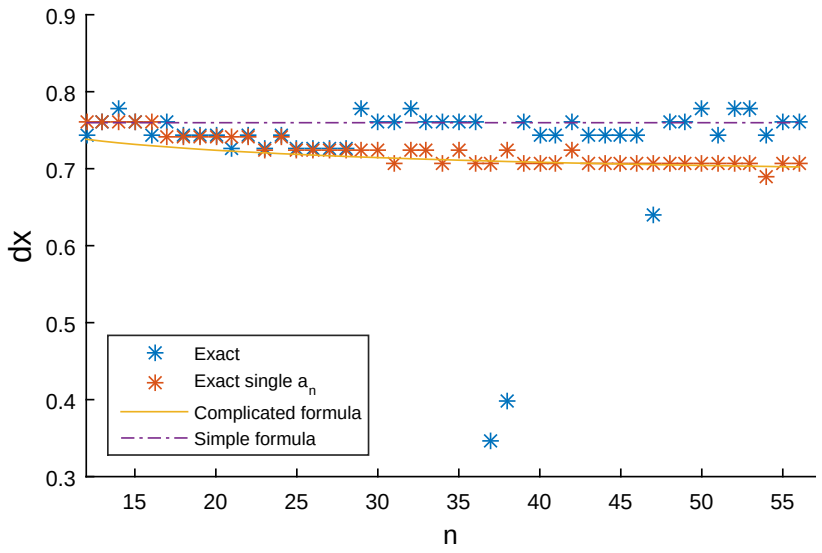

Figure 3.17: The distances between the peaks, dx. *Exact* is the dx calculated between the peaks from the graph of $\sum \mathsf{a_n}$ (blue). *Exact single* $\mathsf{a_n}$ is the dx calculated between the first peaks of the single $\mathsf{a_n}$ (orange). *Simple formula* is the dx calculated by equation (2.8) (purple). *Complicated formula* is the dx calculated by equation (2.9) (yellow) which depends on x and n. For all calculations radius of the sphere $a = 5.5 \times 10^{-6}$m, refractive index $m = 1.48$ and resolution of $\Delta\tilde{\nu} = 5\text{cm}^{-1}$ was used. The numerical values are given in table C.2 in appendix C.

In figure 3.17 the difference between the distance dx from the peaks in $\sum \mathsf{a_n}$

(*Exact*) and from the first order peaks form $\mathsf{a_n}$ (*Exact single* $\mathsf{a_n}$) are large, especially for $n > 30$. Since, *Exact single* $\mathsf{a_n}$(blue) is close to *Complicated formula*(yellow), equation (2.9) which depends on x and n, would be a good approximation for the distance between the peaks for $n > 12$. As n increases, the distance between the first peaks(*Exact single* $\mathsf{a_n}$, orange) are approximated well with the equation (2.9). For $n < 30$ there are occasional overlaps between *Exact single* $\mathsf{a_n}$(orange) and *Exact*(blue). An overlap indicates that the peaks from $\sum \mathsf{a_n}$ (blue) are first order peaks. Because of the large difference between *Exact*(blue) and *Exact single* $\mathsf{a_n}$(orange) it indicates that $\sum \mathsf{a_n}$, employed with $\Delta\tilde{\nu} = 5\text{cm}^{-1}$, does not contain only first order peaks. This confirms what was observed in chapter 3.1.1: when the resolution is low, the visible peaks in $\sum \mathsf{a_n}$ for low n are first order peaks, but as n increases the visible peaks are higher order peaks.

It is interesting to see if equation (2.9) gives a better approximation for the distance between the peaks as n is increased further. In figure 3.17, it is shown that calculations using equation (2.9) gives a better approximation than equation (2.8) for dx from $\mathsf{a_n}$. The distance between the first order peaks from $\mathsf{a_n}$ and the results from the two approximation formulas(*Simple formula* and *Complicated formula*) are plotted in figure 3.18. As this figure illustrates, equation (2.9) gives a very good approximation for high n. *Exact single* $\mathsf{a_n}$ (blue), is very close to *Complicated formula* (yellow) for $n \approx 30$. The positions of the first order peaks for $\mathsf{a_n}$ are computed with high resolution, $\Delta x = 0.01$, which is equivalent to $\Delta\tilde{\nu} = 2.9\text{cm}^{-1}$ calculated by equation (3.1). These results are calculated from $n = 1$ to $n = 60$ in order to see how dx changes as n increases. The numerical results are given in table C.3. The table is generated using the Matlab script $Plot\_different\_deltax\_resultsn1\_60.m$ [14] and the results are displayed in figure 3.18.

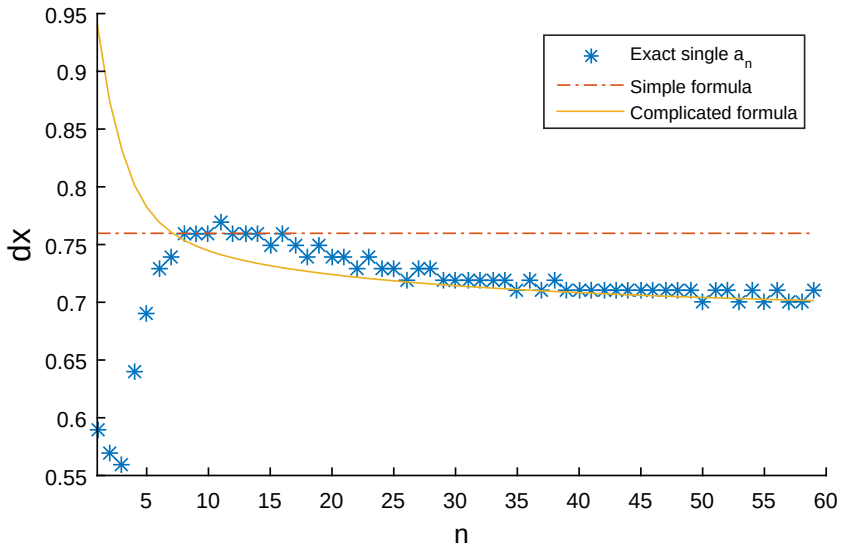

Figure 3.18: The distances between the peaks, dx. *Exact single* $\mathsf{a_n}$ is the dx calculated between the first peaks of the single $\mathsf{a_n}$ (blue). *Simple formula* is the dx calculated by equation (2.8) (orange). *Complicated formula* is the dx calculated by equation (2.9) (yellow) which depends on x and n. For all calculations radius of the sphere $a = 5.5{\times}10^{-6}$m, refractive index $m = 1.48$ and resolution $\Delta x = 0.01$ which is equivalent to $\Delta\tilde{\nu} = 2.9\text{cm}^{-1}$ was used. The results are plotted from $n = 1$ to $n = 60$. The numerical values are given in table C.3 in appendix C.

As the previous figure shows, equation (2.9) (*Complicated formula*), is a good approximation for $n \geq 30$. For $n \leq 30$ the approximation is not very good. In figure 3.19 the area $1 \leq n \leq 15$ is enlarged in order to highlight the difference between *Exact single* $\mathsf{a_n}$ (blue), and *Complicated formula* (yellow). These numerical results are displayed in a separate table, table C.4 in appendix C, which also contains the absolute error. The table is generated using the Matlab script $Plot\_different\_deltax\_resultsn1\_60.m$ [14].

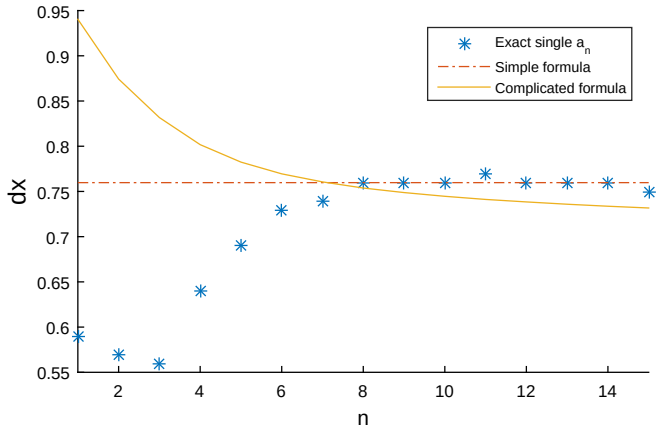

Figure 3.19: The distances between the peaks, dx. *Exact single* $\mathsf{a_n}$ is the dx calculated between the first peaks of the single $\mathsf{a_n}$ (blue). *Simple formula* is the dx calculated by equation (2.8) (orange). *Complicated formula* is the dx calculated by equation (2.9) (yellow) which depends on x and n. For all calculations radius of the sphere $a = 5.5{\times}10^{-6}$m, refractive index $m = 1.48$ and resolution $\Delta x = 0.01$ which is equivalent to $\Delta\tilde{\nu} = 2.9\text{cm}^{-1}$. The results are plotted from $n = 1$ to $n = 15$. The numerical values are given in table C.4 in appendix C.

In the next figures(3.20-3.27) *Exact single* $\mathsf{a_n}$ (blue), *Simple formula* (orange) and *Complicated formula* (yellow) are plotted. The refractive index is changed from $m = 1.3$ to $m = 1.5$, to be able to see how the refractive index alter the results. The resolution for *Exact* is the same, $\Delta x = 0.01$, which is equivalent to a step as small as 2.9cm^{-1} in the wavenumber. In figure 3.20 and 3.21 the refractive index is $m = 1.3$. In figure 3.22 and 3.23 the refractive index is $m = 1.4$. In figure 3.24 and 3.25 the refractive index is $m = 1.46$. In figure 3.26 and 3.27 the refractive index is $m = 1.5$.

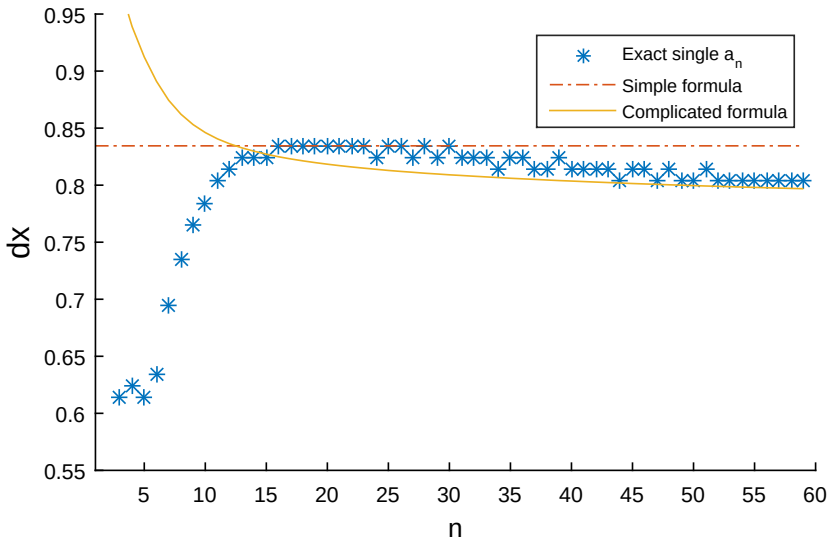

Figure 3.20: The distances between the peaks, dx. *Exact single* $\mathsf{a_n}$ is the dx calculated between the first peaks of the single $\mathsf{a_n}$ (blue). *Simple formula* is the dx calculated by equation (2.8) (orange). *Complicated formula* is the dx calculated by equation (2.9) (yellow) which depends on x and n. For all calculations a radius of the sphere $a = 5.5 \times 10^{-6}$m, a refractive index of $m = 1.3$ and a resolution of $\Delta x = 0.01$ which is equivalent to $\Delta\tilde{\nu} = 2.9\text{cm}^{-1}$. The results are plotted from $n = 1$ to $n = 60$.

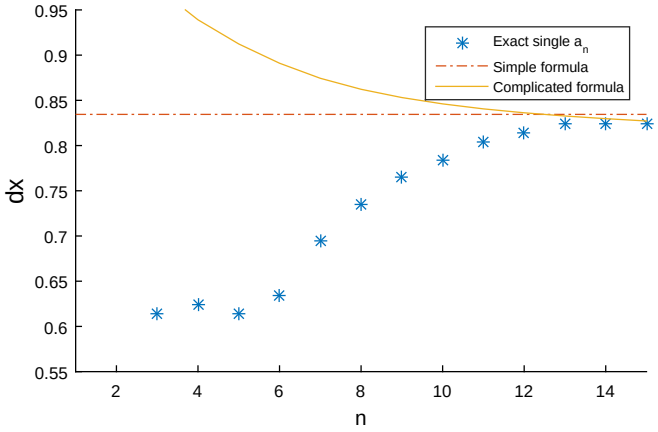

Figure 3.21: The distances between the peaks, dx. *Exact single* $\mathsf{a_n}$ is the dx calculated between the first peaks of the single $\mathsf{a_n}$ (blue). *Simple formula* is the dx calculated by equation (2.8) (orange). *Complicated formula* is the dx calculated by equation (2.9) (yellow) which depends on x and n. For all calculations a radius of the sphere $a = 5.5 \times 10^{-6}$m, a refractive index of $m = 1.3$ and a resolution of $\Delta x = 0.01$ which is equivalent to $\Delta\tilde{\nu} = 2.9\text{cm}^{-1}$. The results are plotted from $n = 1$ to $n = 15$.

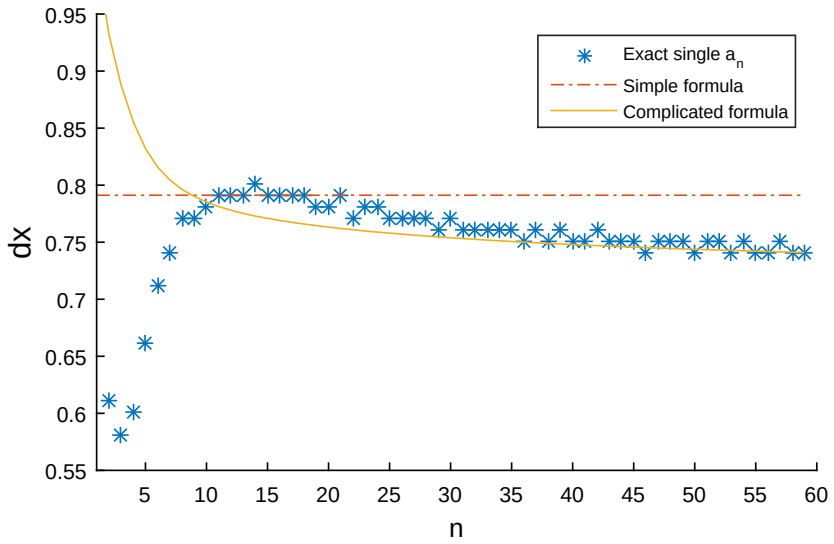

Figure 3.22: The distances between the peaks, dx. *Exact single* $\mathsf{a_n}$ is the dx calculated between the first peaks of the single $\mathsf{a_n}$ (blue). *Simple formula* is the dx calculated by equation (2.8) (orange). *Complicated formula* is the dx calculated by equation (2.9) (yellow) which depends on x and n. For all calculations a radius of the sphere $a = 5.5 \times 10^{-6}$m, a refractive index of $m = 1.4$ and a resolution of $\Delta x = 0.01$ which is equivalent to $\Delta\tilde{\nu} = 2.9\text{cm}^{-1}$. The results are plotted from $n = 1$ to $n = 60$.

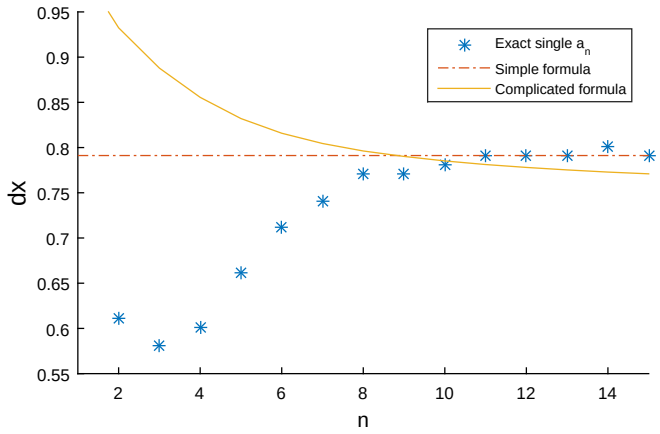

Figure 3.23: The distances between the peaks, dx. *Exact single* $\mathsf{a_n}$ is the dx calculated between the first peaks of the single $\mathsf{a_n}$ (blue). *Simple formula* is the dx calculated by equation (2.8) (orange). *Complicated formula* is the dx calculated by equation (2.9) (yellow) which depends on x and n. For all calculations a radius of the sphere $a = 5.5 \times 10^{-6}$m, a refractive index of $m = 1.4$ and a resolution of $\Delta x = 0.01$ which is equivalent to $\Delta\tilde{\nu} = 2.9\text{cm}^{-1}$. The results are plotted from $n = 1$ to $n = 15$.

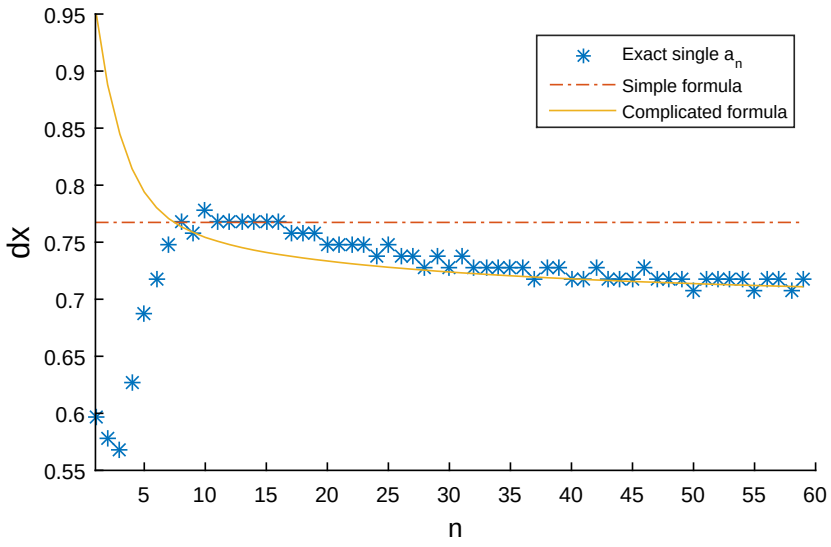

Figure 3.24: The distances between the peaks, dx. *Exact single* $\mathsf{a_n}$ is the dx calculated between the first peaks of the single $\mathsf{a_n}$ (blue). *Simple formula* is the dx calculated by equation (2.8) (orange). *Complicated formula* is the dx calculated by equation (2.9) (yellow) which depends on x and n. For all calculations a radius of the sphere $a = 5.5 \times 10^{-6}$m, a refractive index of $m = 1.46$ and a resolution of $\Delta x = 0.01$ which is equivalent to $\Delta\tilde{\nu} = 2.9\text{cm}^{-1}$. The results are plotted from $n = 1$ to $n = 60$.

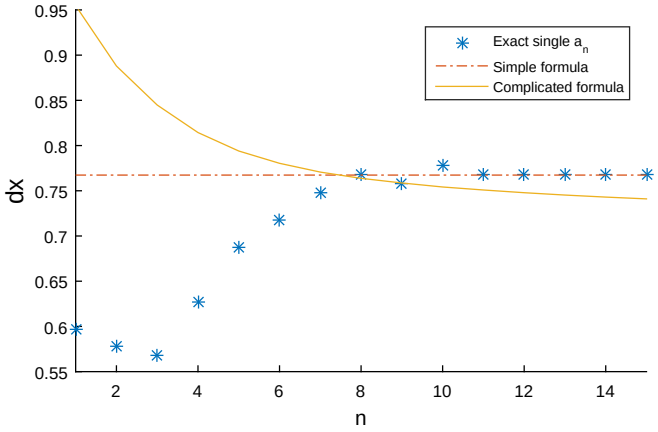

Figure 3.25: The distances between the peaks, dx. *Exact single* $\mathsf{a_n}$ is the dx calculated between the first peaks of the single $\mathsf{a_n}$ (blue). *Simple formula* is the dx calculated by equation (2.8) (orange). *Complicated formula* is the dx calculated by equation (2.9) (yellow) which depends on x and n. For all calculations a radius of the sphere $a = 5.5 \times 10^{-6}$m, a refractive index of $m = 1.46$ and a resolution of $\Delta x = 0.01$ which is equivalent to $\Delta\tilde{\nu} = 2.9\text{cm}^{-1}$. The results are plotted from $n = 1$ to $n = 15$.

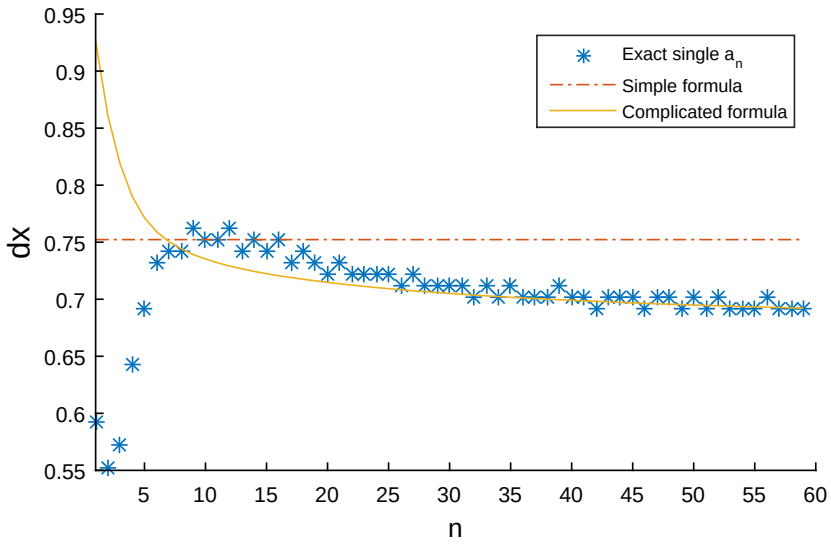

Figure 3.26: The distances between the peaks, dx. *Exact single* $\mathsf{a_n}$ is the dx calculated between the first peaks of the single $\mathsf{a_n}$ (blue). *Simple formula* is the dx calculated by equation (2.8) (orange). *Complicated formula* is the dx calculated by equation (2.9) (yellow) which depends on x and n. For all calculations a radius of the sphere $a = 5.5 \times 10^{-6}$m, a refractive index of $m = 1.5$ and a resolution of $\Delta x = 0.01$ which is equivalent to $\Delta\tilde{\nu} = 2.9\text{cm}^{-1}$. The results are plotted from $n = 1$ to $n = 60$.

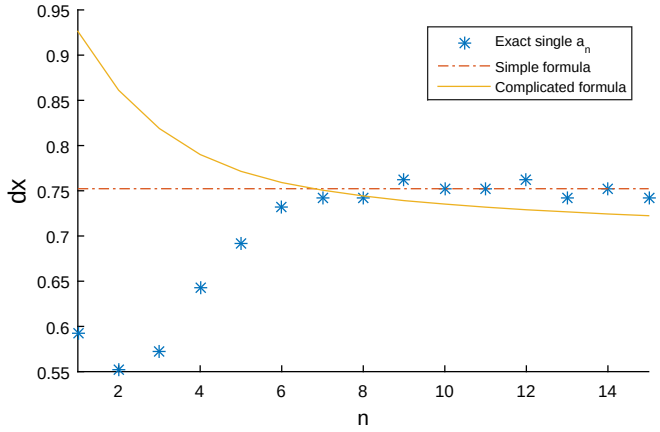

Figure 3.27: The distances between the peaks, dx. *Exact single* $\mathsf{a_n}$ is the dx calculated between the first peaks of the single $\mathsf{a_n}$ (blue). *Simple formula* is the dx calculated by equation (2.8) (orange). *Complicated formula* is the dx calculated by equation (2.9) (yellow) which depends on x and n. For all calculations a radius of the sphere $a = 5.5 \times 10^{-6}$m, a refractive index of $m = 1.5$ and a resolution of $\Delta x = 0.01$ which is equivalent to $\Delta\tilde{\nu} = 2.9\text{cm}^{-1}$. The results are plotted from $n = 1$ to $n = 15$.

As seen in the previous figures, dx-values decrease with m. In addition the intersection between *Simple formula* and *Complicated formula* move from $n = 9$ towards $n = 7$ as m is increased. In chapter 2.3.1 it is stated that equation (2.8) and equation (2.9) hold under the assumptions that $x \gg 1$. This is confirmed in the previous figures. In figure 3.16, *Exact* gets closer to *Simple formula*(orange) as n and with that x increases. In figure 3.17 to figure 3.27 *Exact single* $\mathsf{a_n}$ get closer to *Complicated formula*(yellow), as n and x increases. In other words, equation (2.8) and equation (2.9) are more accurate for $x \gg 1$. It is also seen in the previous figures that, for the area $1 < x < 8$, equation (2.9) does not give a very good estimate for the distance between the resonances. Neither of the two formulas deliver a good estimate in this area. For $n = 8$ to $n = 15$, equation (2.8) certainly is the best approximation. In the area from $1 < n < 8$ it might be necessary to find another way of computing dx.

3.2.2 Using Bisection to Obtain the Refractive Index

In this section bisection is going to be applied to the equations, given in chapter 2.3.1, for calculating the distance between the peaks. The aim is to calculate an estimate for the refractive index from simulated spectra.

Equation (2.8) and equation (2.9), given in chapter 2.3.1, are rearranged on the form $f(m) = 0$

$$dx \cdot (m^2 - 1)^{1/2} - tan^{-1}(m^2 - 1)^{1/2} = 0, \tag{3.2}$$

$$dx \cdot n((mx/n)^2 - 1^{1/2}) - x \cdot tan^{-1}((mx/n)^2 - 1)^{1/2} = 0. \tag{3.3}$$

In the Matlab script *Simulation2.m* [14], bisection is used on equation (3.2) and equation (3.3) to find the zeros. The $\sum \mathsf{a_n}$ is plotted for $11 < n < 34$ and the zeros are calculated with tolerance $\epsilon = 10^{-10}$. The first test of estimating the refractive index from the graph using bisection is implemented with a constant refractive index $m = 1.48$, radius of the sphere 5.5×10^{-6}m and $\Delta\tilde{\nu} = 5\text{cm}^{-1}$. *m graph* is the constant refractive index in the graph, *m simple formula* is the refractive index calculated using bisection on equation (3.2) and *m complicated formula* is the refractive index calculated using bisection on equation (3.3). This result is given in table 3.1.

Table 3.1: Bisection is used on equation (3.2) and equation (3.3) to find the zeros. The first test of estimating the refractive index from the graph using bisection is implemented with a constant refractive index $m = 1.48$ and $\Delta\tilde{\nu} = 5\text{cm}^{-1}$. The $\sum \mathsf{a_n}$ is plotted for $11 < n < 34$ and the zeros are calculated with tolerance $\epsilon = 10^{-10}$. *m graph* is the constant refractive index in the graph, *Simple formula* is the refractive index calculated using bisection on equation (3.2) and *Complicated formula* is the refractive index calculated using bisection on equation (3.3).

Graph	Simple formula	Complicated formula
1.48	1.57462241128087	1.52636288329959
1.48	1.52546649798751	1.46726275011897
1.48	1.4786015547812	1.41274695321918
1.48	1.43387502059341	1.79999999925494
1.48	1.4786015547812	1.40199743285775
1.48	1.52546649798751	1.44360328838229
1.48	1.4786015547812	1.79999999925494
1.48	1.52546649798751	1.43465180322528
1.48	1.52546649798751	1.43048443868756
1.48	1.52546649798751	1.42669081762433
1.48	1.57462241128087	1.47184311524034
1.48	1.52546649798751	1.4194560430944
1.48	1.57462241128087	1.46512661352754
1.48	1.52546649798751	1.41331238821149
1.48	1.57462241128087	1.45938547030091
1.48	1.57462241128087	1.45655974075198
1.48	1.57462241128087	1.45392350777984
1.48	1.57462241128087	1.45145833268762
1.48	1.43387502059341	1.79999999925494
1.48	1.4786015547812	1.79999999925494
1.48	1.4786015547812	1.79999999925494
1.48	1.43387502059341	1.79999999925494
1.48	1.4786015547812	1.79999999925494

From table 3.1 it appears that equation (3.2)(*Simple formula*) gives the best approximation to the refractive index in the graph. To determine how good the approximations are it is necessary to calculate the absolute error. The absolute error is displayed in table 3.2.

Table 3.2: The absolute error for the results from table 3.1.

Simple formula	Complicated formula
0.09	0.05
0.05	0.013
0.0014	0.06
0.05	0.3
0.0014	0.08
0.05	0.04
0.0014	0.3
0.05	0.05
0.05	0.05
0.05	0.05
0.09	0.008
0.05	0.06
0.09	0.015
0.05	0.07
0.09	0.02
0.09	0.02
0.09	0.03
0.09	0.03
0.05	0.3
0.0014	0.3
0.0014	0.3
0.05	0.3
0.0014	0.3

The average absolute error and the maximum absolute error from table 3.2 are displayed in table 3.3.

Table 3.3: Average absolute error and maximum absolute error for the results from table 3.1 when $\Delta\tilde{\nu} = 5\text{cm}^{-1}$.

	Simple formula	Complicated formula
Average absolute error	0.05	0.13
Max absolute error	0.09	0.3

So, as illustrated in table 3.3, the smallest average absolute error is obtained by equation (3.2)(*Simple formula*). The maximum absolute error from this equation is also much smaller than for equation (3.3)(*Complicated formula*). This indicates that when the resolution is low, i.e. $\Delta\tilde{\nu} = 5\text{cm}^{-1}$, as in table 3.1 the simplest formula, equation (3.2), gives the best result.

The zeros of the functions are calculated for resolution $\Delta\tilde{\nu} = 0.2\text{cm}^{-1}$ as well, and these results are given in table 3.4.

Table 3.4: Bisection is used on equation (3.2) and equation (3.3) to find the zeros. The second test of estimating the refractive index from the graph using bisection is implemented with a constant refractive index $m = 1.48$ and $\Delta\tilde{\nu} = 0.2\text{cm}^{-1}$. The $\sum \mathsf{a_n}$ is plotted for $11 < n < 34$ and the zeros are calculated with tolerance $\epsilon = 10^{-10}$. *m graph* is the constant refractive index in the graph, *Simple formula* is the refractive index calculated using bisection on equation (3.2) and *Complicated formula* is the refractive index calculated using bisection on equation (3.3).

Graph	Simple formula	Complicated formula
1.48	1.55073144063354	1.50226842835546
1.48	1.51972487941384	1.46170491501689
1.48	1.47130537852645	1.40574932470918
1.48	1.47312432453036	1.40154795572162
1.48	1.4786015547812	1.40165207609534
1.48	1.49708269312978	1.41514203771949
1.48	1.50645446255803	1.41981669589877
1.48	1.51972487941384	1.42866552993655
1.48	1.52546649798751	1.43027439191937
1.48	1.53124108836055	1.43220162913203
1.48	1.53899231180549	1.43633127436042
1.48	1.54680331274867	1.44071128591895
1.48	1.55073144063354	1.44142100140452
1.48	1.55863337740302	1.44624990895391
1.48	1.56460014209151	1.44929421767592
1.48	1.56859734579921	1.45052758082747
1.48	1.57462241128087	1.45390356704593
1.48	1.57865876033902	1.45542279556394
1.48	1.58271092250943	1.45707283392549
1.48	1.5888190202415	1.46085551902652
1.48	1.5888190202415	1.45868939831853
1.48	1.59496321454644	1.46270601376891
1.48	1.59701935574412	1.46275203749537

The absolute error for the results from table 3.4 are displayed in table 3.5.

Table 3.5: The absolute error for the results from table 3.4.

Simple formula	Complicated formula
0.07	0.02
0.04	0.018
0.009	0.07
0.007	0.08
0.0014	0.08
0.017	0.06
0.03	0.06
0.04	0.05
0.05	0.05
0.05	0.05
0.06	0.04
0.07	0.04
0.07	0.04
0.08	0.03
0.08	0.03
0.09	0.03
0.09	0.03
0.10	0.02
0.10	0.02
0.11	0.019
0.11	0.02
0.11	0.017
0.12	0.017

As shown in table 3.5 the absolute error for the results calculated with equation (3.3)(*Complicated formula*) is smaller than for the results from equation (3.2)(*Simple formula*). The average absolute error and the maximum absolute error for $\Delta\tilde{\nu} = 0.2\text{cm}^{-1}$ are displayed in table 3.6.

Table 3.6: Average absolute error and maximum absolute error for the results from table 3.4 when $\Delta\tilde{\nu} = 0.2\text{cm}^{-1}$.

	Simple formula	Complicated formula
Average absolute error	0.07	0.04
Max absolute error	0.12	0.08

For higher resolution, i.e. $\Delta\tilde{\nu} = 0.2\text{cm}^{-1}$, it seems as equation (3.3)(*Complicated formula*), gives the best approximation.

3.2.3 Distance Between the Peaks for Different Resolutions

When plotting $\sum \mathsf{a_n}$ with different resolutions there is a shift in the positions of the peaks. This is illustrated in chapter 3.1.1. The calculated distance between the peaks, dx, will vary and can therefore give the wrong refractive index m for the spectra. In this section $\sum \mathsf{a_n}$ is employed with a refractive index $m = 1.48$, a radius of the sphere of 5.5×10^{-6}m and plotted with different resolution. The distances between the peaks is then calculated from $\sum \mathsf{a_n}$ for $12 < n < 33$. Bisection is then used to calculate the refractive index from these results.

Table 3.7 shows the different dx obtained when the resolution is changed. Generated with the Matlab script *Plot_an_many_diff_res.m* [14].

Table 3.7: The distance between the peaks, dx, calculated from the $\sum \mathsf{a_n}$ employed with a refractive index $m = 1.48$, a radius of the sphere of 5.5×10^{-6}m, and resolution $\Delta\tilde{\nu} = 0.2\text{cm}^{-1}$, $\Delta\tilde{\nu} = 2\text{cm}^{-1}$ and $\Delta\tilde{\nu} = 5\text{cm}^{-1}$.

n	$\Delta\tilde{\nu} = 0.2\text{cm}^{-1}$	$\Delta\tilde{\nu} = 2\text{cm}^{-1}$	$\Delta\tilde{\nu} = 5\text{cm}^{-1}$
12	0.745060113725357	0.746442414492934	0.742986662573985
13	0.763030023703887	0.767176926006627	0.760265422168731
14	0.7623388733201	0.760265422168731	0.777544181763474
15	0.760265422168731	0.760265422168731	0.760265422168729
16	0.753353918330832	0.753353918330832	0.742986662573987
17	0.749898166411883	0.746442414492934	0.760265422168731
18	0.745060113725351	0.746442414492934	0.742986662573985
19	0.742986662573987	0.746442414492936	0.742986662573987
20	0.740913211422619	0.739530910655038	0.742986662573987
21	0.738148609887457	0.739530910655038	0.725707902979241
22	0.735384008352298	0.73261940681714	0.742986662573987
23	0.734001707584721	0.73261940681714	0.725707902979241
24	0.731237106049559	0.73261940681714	0.742986662573987
25	0.729163654898191	0.73261940681714	0.725707902979241
26	0.727781354130613	0.725707902979241	0.725707902979241
27	0.725707902979245	0.725707902979241	0.725707902979241
28	0.72432560221166	0.725707902979241	0.725707902979241
29	0.722943301444083	0.718796399141347	0.777544181763474
30	0.720869850292715	0.815557452871911	0.760265422168732
31	0.720869850292715	0.767176926006627	0.760265422168729
32	0.718796399141343	0.767176926006627	0.777544181763474
33	0.718105248757556	0.767176926006627	0.760265422168729

The dx-values agree well until $n \approx 30$. For $n > 30$ the dx-values for $\Delta\tilde{\nu} = 2\text{cm}^{-1}$ and $\Delta\tilde{\nu} = 5\text{cm}^{-1}$ are higher than the dx-values calculated with $\Delta\tilde{\nu} = 0.2\text{cm}^{-1}$.

The method from chapter 3.2.2 is applied to the results from table 3.7 in order to calculate the refractive index. Bisection is used on equation (3.2)(*Simple formula*) and equation (3.3)(*Complicated formula*) to see which of the formulas that gives the best result. In table 3.8 the refractive index is calculated by equation (3.2).

Table 3.8: The refractive index is calculated from the results from table 3.7 where the distance between the peaks, dx, is calculated from the $\sum \mathsf{a_n}$. It is employed with a refractive index $m = 1.48$, a radius of the sphere of 5.5×10^{-6}m. Bisection is used on equation (3.2)(*Simple formula*) with resolution $\Delta\tilde{\nu} = 0.2\text{cm}^{-1}$, $\Delta\tilde{\nu} = 2\text{cm}^{-1}$ and $\Delta\tilde{\nu} = 5\text{cm}^{-1}$.

Graph	$\Delta\tilde{\nu} = 0.2\text{cm}^{-1}$	$\Delta\tilde{\nu} = 2\text{cm}^{-1}$	$\Delta\tilde{\nu} = 5\text{cm}^{-1}$
1.48	1.51972487941384	1.51591531708837	1.52546649798751
1.48	1.47130537852645	1.46046241298318	1.4786015547812
1.48	1.47312432453036	1.4786015547812	1.43387502059341
1.48	1.4786015547812	1.4786015547812	1.4786015547812
1.48	1.49708269312978	1.49708269312978	1.52546649798751
1.48	1.50645446255803	1.51591531708837	1.4786015547812
1.48	1.51972487941384	1.51591531708837	1.52546649798751
1.48	1.52546649798751	1.51591531708837	1.52546649798751
1.48	1.53124108836055	1.53510927036405	1.52546649798751
1.48	1.53899231180549	1.53510927036405	1.57462241128087
1.48	1.54680331274867	1.5546747662127	1.52546649798751
1.48	1.55073144063354	1.5546747662127	1.57462241128087
1.48	1.55863337740302	1.5546747662127	1.52546649798751
1.48	1.56460014209151	1.5546747662127	1.57462241128087
1.48	1.56859734579921	1.57462241128087	1.57462241128087
1.48	1.57462241128087	1.57462241128087	1.57462241128087
1.48	1.57865876033902	1.57462241128087	1.57462241128087
1.48	1.58271092250943	1.59496321454644	1.43387502059341
1.48	1.5888190202415	1.59999999925494	1.4786015547812
1.48	1.5888190202415	1.46046241298318	1.4786015547812
1.48	1.59496321454644	1.46046241298318	1.43387502059341
1.48	1.59701935574412	1.46046241298318	1.4786015547812

In table 3.9 the refractive index is calculated by equation (3.3)(*Complicated formula*).

Table 3.9: The refractive index is calculated from the results from table 3.7 where the distance between the peaks, dx, is calculated from the $\sum \mathsf{a_n}$. It is employed with a refractive index $m = 1.48$, a radius of the sphere of 5.5×10^{-6}m. Bisection is used on equation (3.3)(*Complicated formula*) with resolution $\Delta\tilde{\nu} = 0.2\text{cm}^{-1}$, $\Delta\tilde{\nu} = 2\text{cm}^{-1}$ and $\Delta\tilde{\nu} = 5\text{cm}^{-1}$.

Graph	$\Delta\tilde{\nu} = 0.2\text{cm}^{-1}$	$\Delta\tilde{\nu} = 2\text{cm}^{-1}$	$\Delta\tilde{\nu} = 5\text{cm}^{-1}$
1.48	1.46170491501689	1.45776949450374	1.46726275011897
1.48	1.40574932470918	1.79999999925494	1.41274695321918
1.48	1.40154795572162	1.40711383447051	1.79999999925494
1.48	1.40165207609534	1.40168348774314	1.40199743285775
1.48	1.41514203771949	1.41517197266221	1.44360328838229
1.48	1.41981669589877	1.42921665981412	1.79999999925494
1.48	1.42866552993655	1.42478423044085	1.43465180322528
1.48	1.43027439191937	1.42076982185245	1.43048443868756
1.48	1.43220162913203	1.43610419258475	1.42669081762433
1.48	1.43633127436042	1.43251553401351	1.47184311524034
1.48	1.44071128591895	1.44856401607394	1.4194560430944
1.48	1.44142100140452	1.44529563263059	1.46512661352754
1.48	1.44624990895391	1.44227311238647	1.41331238821149
1.48	1.44929421767592	1.43946972563863	1.45938547030091
1.48	1.45052758082747	1.45655974075198	1.45655974075198
1.48	1.45390356704593	1.45392350777984	1.45392350777984
1.48	1.45542279556394	1.45145833268762	1.45145833268762
1.48	1.45707283392549	1.46922078803182	1.79999999925494
1.48	1.46085551902652	1.79999999925494	1.79999999925494
1.48	1.45868939831853	1.79999999925494	1.79999999925494
1.48	1.46270601376891	1.79999999925494	1.79999999925494
1.48	1.46275203749537	1.79999999925494	1.79999999925494

The average and absolute error from the results in table 3.9 and table 3.8 is displayed in table 3.10.

Table 3.10: Average absolute error and maximum absolute error for the results from table 3.8 and table 3.9.

	Simple formula	Complicated formula
Average absolute error $\Delta\tilde{\nu} = 0.2\text{cm}^{-1}$	0.07	0.04
Max absolute error $\Delta\tilde{\nu} = 0.2\text{cm}^{-1}$	0.12	0.08
Average absolute error $\Delta\tilde{\nu} = 2\text{cm}^{-1}$	0.05	0.11
Max absolute error $\Delta\tilde{\nu} = 2\text{cm}^{-1}$	0.12	0.3
Average absolute error $\Delta\tilde{\nu} = 5\text{cm}^{-1}$	0.05	0.13
Max absolute error $\Delta\tilde{\nu} = 5\text{cm}^{-1}$	0.09	0.3

For resolution $\Delta\tilde{\nu} = 0.2\text{cm}^{-1}$, the smallest average absolute error are obtained

by equation (3.3)(*Complicated formula*). For higher resolution, $\Delta\tilde{\nu} = 2\text{cm}^{-1}$ and $\Delta\tilde{\nu} = 5\text{cm}^{-1}$, the average absolute error are small when using equation (3.2)(*Simple formula*).

3.3 Identifying Peak Order and Index in $\sum \mathsf{a_n}$

In figure 3.28, $\sum \mathsf{a_n}$ is plotted with constant refractive index $m = 1.48$, radius of the sphere $a = 5.5 \times 10^{-6}\text{m}$ and resolution $\Delta\tilde{\nu} = 5\text{cm}^{-1}$. The peaks are numbered from 12 to 57, starting at $n = 12$ because this peak is equivalent to the first peak of a_{12} in figure 3.10. It is then assumed that the following peaks are successive peaks. The positions for the peaks in $\sum \mathsf{a_n}$ are found using the Matlab script *Plot_An_save_peaks_table.m* [14] and saved in table 3.12.

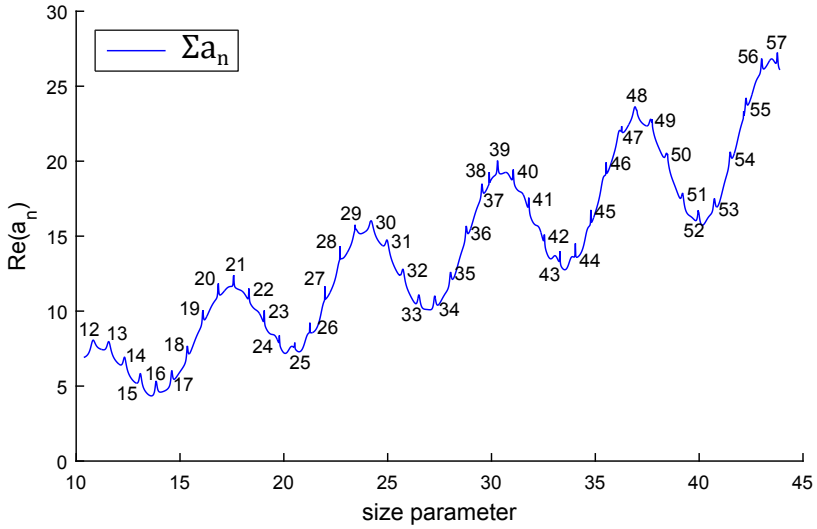

Figure 3.28: $\sum \mathsf{a_n}$ with radius of the sphere $a = 5.5 \times 10^{-6}\text{m}$, refractive index $m = 1.48$ and resolution $\Delta\tilde{\nu} = 5\text{cm}^{-1}$. The peaks are numbered from 12 to 57.

The position of the first, second and third order peaks for $1 < n < 50$ for each $\mathsf{a_n}$ are found using the Matlab script *table_single_an_peak_locations.m* [14]. Each $\mathsf{a_n}$ is plotted with constant refractive index $m = 1.48$ and resolution $\Delta x = 0.005$ which corresponds to $\Delta\tilde{\nu} = 1.45\text{cm}^{-1}$, according to equation (3.1). The x-coordinate for each peak is given in table 3.11. This table can be used to decide if the peaks located in $\sum \mathsf{a_n}$ with resolution $\Delta\tilde{\nu} = 5\text{cm}^{-1}$ are first, second or third peaks. The coordinates in table 3.12 can be compared to the coordinates in table 3.11. Thus, it will be possible to decide if the peaks are first, second or third order peaks.

Table 3.11: The positions of the first, second and third order peaks for each $\mathsf{a_n}$ with constant refractive index $m = 1.48$ and $\Delta x = 0.005$.

n	1. peak	2. peak	3. peak
1	3.245	9.665	16.115
2	3.839	10.274	16.719
3	4.404	9.909	16.224
4	4.974	10.319	16.734
5	5.608	10.918	17.303
6	6.298	11.433	16.868
7	7.028	11.628	17.383
8	7.773	11.923	17.983
9	8.527	12.447	18.387
10	9.287	13.017	18.257
11	10.047	13.592	18.747
12	10.812	14.167	19.332
13	11.576	14.751	19.906
14	12.336	15.371	20.421
15	13.091	16.031	20.851
16	13.851	16.721	21.296
17	14.600	17.430	21.810
18	15.350	18.155	22.375
19	16.095	18.895	22.955
20	16.840	19.645	23.535
21	17.579	20.399	24.104
22	18.319	21.159	24.679
23	19.054	21.919	25.264
24	19.788	22.683	25.883
25	20.518	23.448	26.538
26	21.248	24.213	27.213
27	21.978	24.978	27.913
28	22.702	25.742	28.627
29	23.427	26.502	29.357
30	24.152	27.267	30.092
31	24.872	28.027	30.837
32	25.591	28.781	31.586
33	26.311	29.541	32.341
34	27.031	30.296	33.096
35	27.746	31.046	33.856
36	28.460	31.795	34.620
37	29.175	32.545	35.385
38	29.890	33.290	36.145
39	30.605	34.035	36.915
40	31.319	34.779	37.679
41	32.029	35.524	38.444
42	32.744	36.264	39.204
43	33.453	37.003	39.968
44	34.163	37.738	40.728
45	34.873	38.478	41.493
46	35.583	39.213	42.253
47	36.292	39.947	43.007
48	36.997	40.677	43.767
49	37.707	41.412	44.522
50	38.412	42.142	45.277

Table 3.12: The positions of the peaks for $\sum \mathsf{a_n}$ employed with constant refractive index $m = 1.48$, radius of the sphere $a = 5.5 \times 10^{-6}$m and $\Delta\tilde{\nu} = 5\text{cm}^{-1}$.

nr	x - coordinates
12	10.8165035063097
13	11.5594901688836
14	12.3197555910524
15	13.0972997728158
16	13.8575651949846
17	14.6005518575586
18	15.3608172797273
19	16.1038039423013
20	16.8467906048753
21	17.5897772674493
22	18.3154851704285
23	19.0584718330025
24	19.7841797359817
25	20.5271663985557
26	21.252874301535
27	21.9785822045142
28	22.7042901074934
29	23.4299980104727
30	24.2075421922362
31	24.9678076144049
32	25.7280730365736
33	26.5056172183371
34	27.2658826405058
35	28.0261480626745
36	28.7864134848433
37	29.546678907012
38	29.8922540989069
39	30.289665569586
40	31.0499309917547
41	31.7929176543287
42	32.5359043169027
43	33.2961697390714
44	34.0391564016454
45	34.7821430642194
46	35.5251297267934
47	36.2681163893674
48	36.9074304943729
49	37.6676959165416
50	38.4279613387104
51	39.2055055204738
52	39.9484921830478
53	40.7260363648113
54	41.5035805465748
55	42.2465672091487
56	43.0068326313175
57	43.7670980534862

The results fromlooking up the values from table 3.12 in table 3.11 are shown in table 3.13 and illustrated in figure 3.29.

Table 3.13: The results from looking up the values from table 3.12 in table 3.11.

nr	peak order
12-29	1.
38	1.
50	1.
30-37	2.
39-47	2.
48	3.
49	3.

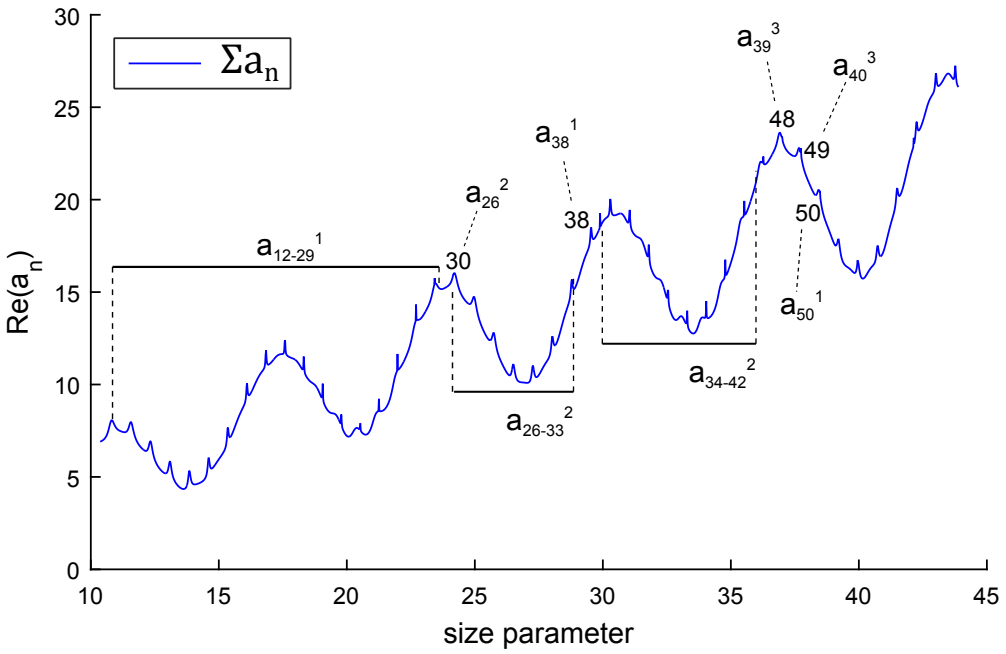

Figure 3.29: Graphical illustration of the results from looking up the values from table 3.12 in table 3.11.

When generating $\sum a_n$ with $\Delta\tilde{\nu} = 5\text{cm}^{-1}$ the peaks are not of the same order. To be able to correctly determine the refractive index using the approximation formulas from chapter 2.3.1, it is necessary to take the difference between the successive peaks. This problem is illustrated, in figures 3.16 and 3.17, in chapter

3.2.1. Three outliers are visible in figure 3.16 and with this method, it is now possible to determine the reason for these outliers. The outliers are caused by calculating the distance between peak 37-38, 38-39, and 47-48 in figure 3.28. When calculating the distance between these peaks using the x-coordinates from table 3.12 the dx values corresponds to the outliers in figure 3.16. This deviation from the other calculated dx- values is explained when taking a closer look at table 3.12 and table 3.11. The x-coordinates for the peak at 38 is equivalent to $\mathsf{a}_{38}{}^{1}$, 37 is equivalent to $\mathsf{a}_{33}{}^{2}$, 39 is equivalent to $\mathsf{a}_{34}{}^{2}$, 47 is equivalent to $\mathsf{a}_{42}{}^{2}$ and 48 is equivalent to $\mathsf{a}_{39}{}^{3}$. As seen in figure 3.16 in chapter 3.2.1, dx lies around between 0.7 and 0.8. When looking at the values in table 3.14 it becomes clear that these values are responsible for the outliers.

Table 3.14: Peaks 38 → 37, 38 → 39 and 47 → 48 with the corresponding correct peak notation and the calculated dx.

Peaks	Corresponds to	dx- value
38-37	$\mathsf{a}_{38}{}^{1} - \mathsf{a}_{33}{}^{2}$	0.3455
39-38	$\mathsf{a}_{34}{}^{2} - \mathsf{a}_{38}{}^{1}$	0.3974
48-47	$\mathsf{a}_{39}{}^{3} - \mathsf{a}_{42}{}^{2}$	0.6393

3.4 Effect of the Dispersive Refractive Index on Q_{ext}

For future work, it is of interest to see if it is possible to adjust the simulated spectra of Q_{ext} to experimental spectra from PMMA spheres or pollen grains. From the experimental spectra of PMMA spheres the radius of the sphere is known, so the only adjustable parameter is the refractive index.

In figure 3.1, 3.2 and 3.3 the refractive index m is constant. In figure 3.30 the extinction efficiency is generated for a sphere with radius $a = 5.5 \times 10^{-6}$m using a dispersive refractive index and constant resolution $\Delta\tilde{\nu} = 5\text{cm}^{-1}$. The refractive index is changed from $m = 1.4$ to $m = 1.7$ along the whole spectral region. For comparison, an extinction efficiency with constant refractive index $m = 1.4$ is plotted in the same figure. When we assume a dispersive refractive index, m changing with the wavenumber, we can notice large changes in the background oscillations for a small change in the refractive index. Figure 3.30 is generated using the Matlab script *Plot_many_Qext_changing_refractive_index.m* [14].

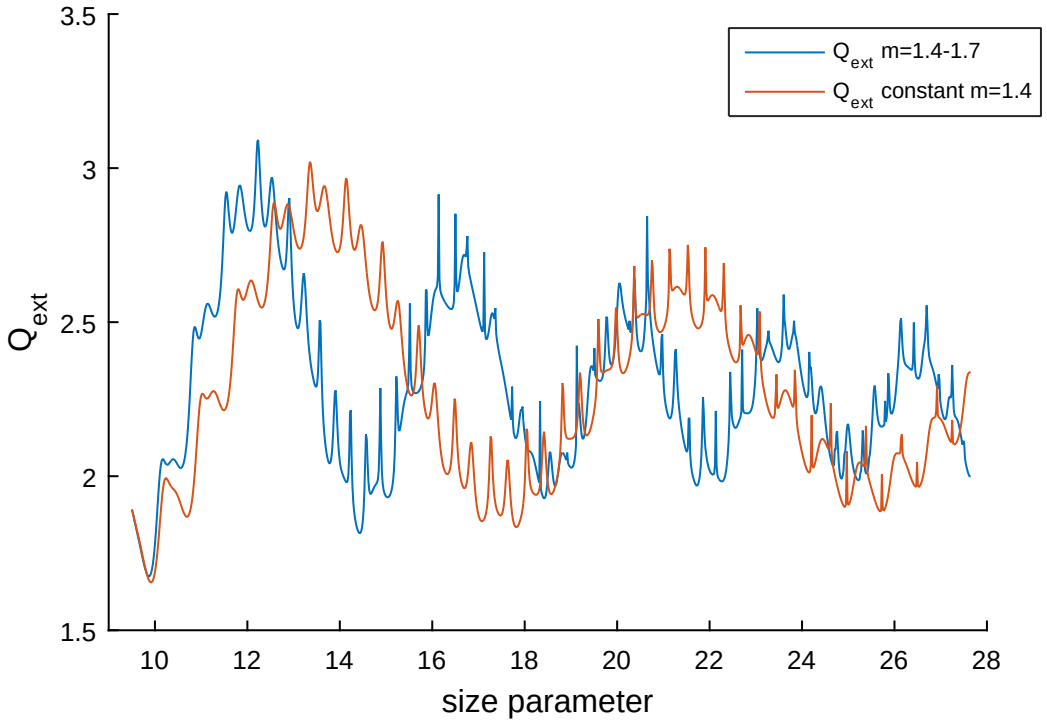

Figure 3.30: Plot of two Q_{ext} with radius $a = 5.5 \times 10^{-6}$m and resolution $\Delta\tilde{\nu} = 5\text{cm}^{-1}$ on the interval $9 < x < 28$. Dispersive refractive index from $m = 1.4$ to $m = 1.7$ (blue) and constant refractive index $m = 1.4$ (orange).

Chapter 4

Discussion

Petr Chỳlek suggested two formulas for the approximation of the distance between the resonances in the ripple structures as a function of the refractive index [6, 7]. Since, in infrared microspectroscopy, spectra of small spheres, i.e. with sizes in the same order as the wavelength of the infrared light, can be obtained, these approximation formulas could be used for the estimation of the refractive index in the infrared region of the electromagnetic spectrum. Different aspects, such as resolution, formula accuracy, resonance order, and resonance index need to be taken into account when evaluating these formulas. In chapter 3.2.2 it was shown that when a low resolution was employed, i.e. $\Delta\tilde{\nu} = 5\text{cm}^{-1}$, the best results were obtained solving equation (3.2) by bisection. For high resolution, i.e. $\Delta\tilde{\nu} = 0.2\text{cm}^{-1}$, the best results were obtained when solving equation (3.3) by bisection. Thus, the resolution of the simulated spectra has an impact on which of the approximation formulas that should be used.

In chapter 3.2.1 it is shown that when calculating the distance between the resonances using Petr Chỳlek formulas, given in chapter 2.3.1, from $\sum \mathsf{a_n}$ generated with $\Delta\tilde{\nu} = 5\text{cm}^{-1}$, equation (2.8) gives the most accurate result for $n > 30$. For $n < 30$, equation (2.9) give the most accurate result for the distances between the peaks in $\sum \mathsf{a_n}$. The best estimate for the distance dx between the first order peaks from each $\mathsf{a_n}$ is obtained by equation (2.9). For both approximation formulas, certain ranges of validity were given by Petr Chỳlek [6, 7]. Equation (2.8) and equation (2.9) were defined to hold under the assumptions $x \gg 1$, $n \gg 1$, $\frac{x}{n} \sim 1$ and $mx \sim n$. In addition, the distance dx between the resonances has to be calculated between successive peaks; n and $n+1$. In chapter 3.1.1, single $\mathsf{a_n}$ is plotted from $n = 8$ to $n = 34$. For this range the assumption $\frac{x}{n} \sim 1$ is determined to be valid by observation, the peak with index n is located close to position $x = n$. From figure 3.18 to figure 3.27 in chapter 3.2.1 the range of validity, the assumption that $n \gg 1$, for the approximation formulas is visible: Equation

(2.8) and equation (2.9) delivers a bad approximation for $n < 10$, but a good approximation for $n > 10$. So, for this area, $n < 10$, the distance between the peaks should be calculated otherwise. One option for $n < 10$ is to calculate the distance between the first order peaks for the single $\mathsf{a_n}$. The distance between the resonances was also calculated for different refractive indices to see if it affected the results. For a low refractive index, i. e. $m = 1.3$, equation (2.8) provide a good approximation for the area $15 < n < 40$, while equation (2.9) approximate the area $40 < n < 60$ well. For high refractive index, i.e. $m = 1.5$, a good approximation for dx is provided by equation (2.9) for the area $20 < n < 60$. The area $10 < n < 20$ is approximated well by equation (2.8). For calculating dx for different refractive indices it can be useful to take this into account since the accuracy of the formulas differ for different ranges of n in addition to for different ranges of the refractive index m.

Since Petr Chỳlek's formulas [6, 7] contained the refractive index m as a variable it was interesting to explore if these equations could be rearrange such that they could be used for estimating the refractive index. Bisection was used to estimate a dispersive refractive index that change with the wavenumber for different resolutions applying a tolerance of $\epsilon = 10^{-10}$. The accuracy of the estimation of the refractive index by bisection depends further on the resolution that can be achieved in a given experimental setup. Since equation (3.3) takes into account the position and index of the peak when calculating the distance dx, one would assume this formula gave the most accurate result for the refractive index for any resolution. This is, as shown in chapter 3.2.2, not the case. The equation that gives the best estimate for the refractive index depends on which resolution that is employed. For a resolution of $\Delta\tilde{\nu} = 0.2\text{cm}^{-1}$ and $m = 1.48$, equation (3.3) gives the most accurate estimate for the refractive index with maximum absolute error estimated to 0.08. Thus, equation (3.3) gives a good approximation for the refractive index when the resolution is high. Using a resolution of $\Delta\tilde{\nu} = 5\text{cm}^{-1}$ and a refractive index of $m = 1.48$, the best estimate for the refractive index was obtained by applying bisection on equation (3.2). The maximum absolute error was estimated to 0.09, thus, equation (3.2) gives a good approximation to the refractive when a resolution that is typical for infrared microspectroscopy is used.

When investigating the different validity ranges of the approximation formulas for the resonance index, it turned out that the resolution has a strong effect on the resonance structure. It affects both the shape of the ripple structure, the number of visible peaks, and the sharpness of the peaks. Further it has an impact on if first order or higher order peaks are visible in the ripple structure. Using a resolution of $\Delta\tilde{\nu} = 5\text{cm}^{-1}$ the peaks in the ripple structure in $\sum \mathsf{a_n}$ are not

only given by first order peaks, as shown in Chapter 3.1.1. It is therefore difficult to decide when calculating distances between peaks in experimentally obtained spectra, if the respective peaks are first or second order peaks. In Chapter 3.3, the order of the peaks in $\sum \mathsf{a_n}$ was determined and displayed graphically. A graphical control of the peak order is necessary when evaluating experimentally obtained spectra. This information needs to be available when fitting simulated Q_{ext} to spectra from PMMA spheres or pollen grains in order to estimate the refractive index.

In chapter 3.1.1 it was determined which peak in $\sum \mathsf{a_n}$ that corresponds to a^1_{11} for resolution $\Delta\tilde{\nu} = 5\text{cm}^{-1}$ and $\Delta\tilde{\nu} = 0.2\text{cm}^{-1}$. It was then assumed that the following peaks were successive peaks. In chapter 3.3 it was established that the peaks in $\sum \mathsf{a_n}$ with resolution $\Delta\tilde{\nu} = 5\text{cm}^{-1}$ did not follow this assumption. The peaks was not all successive peaks, and the order of the peaks varied for this resolution. This has on the other hand, not been assessed for resolution $\Delta\tilde{\nu} = 0.2\text{cm}^{-1}$. Following this assumption, the index employed into equation (3.3), for resolution $\Delta\tilde{\nu} = 5\text{cm}^{-1}$, is not necessarily the correct index for the concerned peak. This might be the reason that equation (3.2) give a better result for $\Delta\tilde{\nu} = 5\text{cm}^{-1}$.

Chapter 5

Conclusion and Outlook

In this thesis the applicability of Petr Chỳlek's approximation formulas [6, 7] for the estimation of the refractive index from spectra was evaluated. Since the validity of the approximation formulas depends both on the index and the order of the resonances, different ranges of the resonance index were considered. Further, the resolution of the scattering extinction turned out to be essential for the appearance of certain resonances. Petr Chỳlek's approximation formulas [6, 7] for the distance dx between the resonances, given in chapter 2.3.1, are not very accurate for estimating the distance between the peaks, dx, in the range $0 < n \lesssim 8$. Equation (2.9), which take the index and the location of the peak into account, gives the best estimate for dx for $n > 30$. Equation (2.8), which is only dependent on the refractive index, gives the best estimate for the distance between the peaks for $8 < n < 20$.

Considering the sum of the electromagnetic modes, $\sum \mathsf{a_n}$, it became apparent that a low resolution, i.e. $\Delta\tilde{\nu} = 5\text{cm}^{-1}$, and employing bisection on equation (3.2), resulted in the the best estimate for the refractive index. For higher resolution, i.e. $\Delta\tilde{\nu} = 0.2\text{cm}^{-1}$, bisection on equation (3.3), resulted in the best estimate for the refractive index.

Outlook

Bisection combined with Petr Chỳlek's formulas, given in chapter 2.3.1, can be used to estimate the real refractive index from the ripple structure in $\sum \mathsf{a_n}$. This method estimates a dispersive real refractive index that change with the wavenumber.

This method can be combined with the method developed by Lukacs et al. [10] where the imaginary part of the refractive index, $\tilde{n}'$, is determined. In this method an accurate estimate of the real part of the complex refractive index is necessary to obtain a good estimate of $\tilde{n}'$. Before the method using bisection can

be combined with other methods it has to be tested on spectra with a dispersive refractive index to determine how accurate it can estimate the real refractive index.

This method then has to be adapted to work on the extinction efficiency, Q_{ext}. Then, combined with the method developed by Lukacs et al. [10], it can give a good estimate for the complex refractive index. Finally, it can then be applied to spectra from PMMA spheres and then to spectra from pollen grains.

Another method that is worth developing further is to work with extinction efficiency from PMMA spheres, and adjust the simulated extinction efficiency, Q_{ext} using the refractive index. The aim would be to adjust the simulated Q_{ext} such that it is as close to the experimental extinction efficiency as possible.

The extinction efficiency has to be adjusted so that two peaks in Q_{ext} are as close to two peaks in the experimental extinction efficiency as possible. This adjustment is done by changing the refractive index of the sphere in the Q_{ext}. The radius of the sphere from the experimental spectra is given. As seen in Chapter 3.4, when the refractive index is changed, it affects the shape of the curve for the extinction efficiency. This observation can be used when trying to adjust the simulated spectra, Q_{ext} to the experimental extinction efficiency. When two peaks are very close, one can assume that the right m is chosen. This refractive index can then be saved. The next step is then to adjust the next two peaks, save this m and so on.

When this method is developed for PMMA spheres it should then be adapted to spectra from pollen grains.

Bibliography

[1] Paul Bassan, Hugh J. Byrne, Franck Bonnier, Joe Lee, Paul Dumas, and Peter Gardner. Resonant mie scattering in infrared spectroscopy of biological materials - understanding the 'dispersion artefact'. *Analyst*, 134:1586–1593, 2009.

[2] Paul Bassan and Peter Gardner. Scattering in biomedical infrared spectroscopy. In *Biomedical Applications of Synchrotron Infrared Microspectroscopy: A Practical Approach*, chapter 8, pages 260–276. The Royal Society of Chemistry, 2011.

[3] Paul Bassan, Achim Kohler, Harald Martens, Joe Lee, Hugh J. Byrne, Paul Dumas, Ehsan Gazi, Michael Brown, Noel Clarke, and Peter Gardner. Resonant mie scattering (rmies) correction of infrared spectra from highly scattering biological samples. *Analyst*, 135:268–277, 2010.

[4] Paul Bassan, Achim Kohler, Harald Martens, Joe Lee, Edward Jackson, Nicholas Lockyer, Paul Dumas, Michael Brown, Noel Clarke, and Peter Gardner. Rmies-emsc correction for infrared spectra of biological cells: Extension using full mie theory and gpu computing. *Journal of Biophotonics*, 3(8-9).

[5] Craig F. Bohren and Donald R. Huffman. *Absorption and scattering of light by small particles*, pages 82–103,289. John Wiley & Sons, 2008.

[6] Petr Chỳlek. Partial-wave resonances and the ripple structure in the mie normalized extinction cross section. *JOSA*, 66(3):285–287, 1975.

[7] Petr Chỳlek. Resonance structure of mie scattering: distance between resonances. *JOSA A*, 7(9):1609–1613, 1990.

[8] Postdoc at NMBU Dr. Rozalia Lukacs. rozalia.lukacs@nmbu.no.

[9] A. Kohler, J. Sulé-Suso, G. D. Sockalingum, M. Tobin, F. Bahrami, Y. Yang, J. Pijanka, P. Dumas, M. Cotte, D. G. van Pittius, G. Parkes, and

H. Martens. Estimating and correcting mie scattering in synchrotron-based microscopic fourier transform infrared spectra by extended multiplicative signal correction. *Appl. Spectrosc.*, 62(3):259–266, 2008.

[10] R. Lukacs, R. Blümel, B. Zimmerman, M. Bağcoiğlu, and A. Kohler. Recovery of absorbance spectra of micrometer-sized biological and inanimate particles. *Analyst*, 140:3273–3284, 2015.

[11] Gustav Mie. Beiträge zur optik trüber medien, speziell kolloidaler metallösungen. *Annalen der Physik*, 330(3):377–445, 1908.

[12] Brian Mohlenhoff, Melissa Romeo, Max Diem, and Bayden R. Wood. Mie-type scattering and non-beer-lambert absorption behavior of human cells in infrared microspectroscopy. *Biophysical Journal*, 88(5):3635 – 3640, 2005.

[13] John M. Stone. *Radiation and optics: an introduction to classical theory*, pages 334–378. McGraw-Hill, 1963.

[14] Nora Thøgersen. Code can be obtained upon request. norathogersen@gmail.com.

[15] Georgi P Tolstov. *Fourier series*, pages 197–208. Courier Corporation, 1962.

[16] Hendrik C. van de Hulst. *Light scattering by small particles*, page 13. John Wiley & Sons, 1957.

[17] Thomas van Dijk, David Mayerich, P. Scott Carney, and Rohit Bhargava. Recovery of absorption spectra from fourier transform infrared (ft-ir) microspectroscopic measurements of intact spheres. *Appl. Spectrosc.*, 67(5):546–552, 2013.

[18] Zhu-Xi Wang, Dun Ren Guo, and XJ Xia. *Special functions*, pages 345–380. World Scientific, 1989.

Appendix A

Bessel Functions

This section is partly based on the book by Tolstov [15].

A.1 Introduction to Bessel Functions

The Bessel equation is the second order differential equation

$$\frac{d^2y}{dx^2} + \frac{1}{x}\frac{dy}{dx} + \left(1 - \frac{p^2}{x^2}\right) y = 0, \tag{A.1.1}$$

where p is the order of the equation. Solutions of equation (A.1.1) are called Bessel functions. Equation (A.1.1) is linear and the general solution can therefore be expressed as

$$y = C_1 y_1 + C_2 y_2, \tag{A.1.2}$$

where C_1 and C_2 are arbitrary constants and y_1 and y_2 are linearly independent particular solutions of equation (A.1.1) [15].

A.2 First, Second and Third Kind

The Bessel functions are divided into three; the first, the second and the third kind. The first kind are denoted $J_p(x)$ and a general expression for the Bessel function of the first kind for all real p is

$$J_{\pm p}(x) = \sum_{m=0}^{\infty} \frac{(-1)^m (x/2)^{\pm p+2m}}{\Gamma(m+1)\Gamma(\pm p + m + 1)}, \tag{A.2.1}$$

where Γ is the gamma- function [15].

When p is not an integer, the Bessel function of second kind is given by

$$Y_p(x) = \frac{J_p(x)cos(p\pi) - J_{-p}(x)}{sin(p\pi)}. \tag{A.2.2}$$

When p is an integer equation (A.2.2) is indeterminate. By applying the l'Hospital rule for $Y_p(x)$ in case of integer $p = n$ [15]

$$\begin{aligned} Y_n(x) = \frac{2}{\pi}J_n(x)\left[ln\left(\frac{x}{2}\right) + C\right] - \frac{1}{\pi}\sum_{m=0}^{n-1}\frac{(n-m-1)!}{m!}\left(\frac{x}{2}\right)^{-n+2m} \\ - \frac{1}{\pi}\sum_{m=0}^{\infty}\frac{(-1)^m(x/2)^{n+2m}}{m!(n+m)!}\left[\sum_{k=1}^{n+m}\frac{1}{k} + \sum_{k=1}^{m}\frac{1}{k}\right]. \end{aligned} \tag{A.2.3}$$

Bessel functions of the second kind are often denoted by the symbol N_p and called Neumann functions.

The third kind of the Bessel functions, which are a linear combination of the first and second kind, are also commonly known as Hankel functions

$$H_p^{(1)}(x) = J_p(x) + iY_p(x), \qquad H_p^{(2)}(x) = J_p(x) - iY_p(x). \tag{A.2.4}$$

Subscript (1) and (2) indicates the first and the second kind of the Hankel functions [18].

A.2.1 Recurrence Relations

Relation between Bessel functions of different orders

$$\begin{aligned} \frac{d}{dx}(x^pJ_p(x)) &= \frac{d}{dx}\sum_{m=0}^{\infty}\frac{(-1)^m x^{2p+2m}}{2^{p+2m}\Gamma(m+1)\Gamma(p+m+1)} \\ &= \sum_{m=0}^{\infty}\frac{(-1)^m x^{2p+2m-1}}{2^{p+2m-1}\Gamma(m+1)\Gamma(p+m)} \\ &= x^pJ_{p-1}(x). \end{aligned}$$

The same holds for $-p$

$$\frac{d}{dx}(x^{-p}J_p(x)) = -x^{-p}J_{p+1}(x).$$

The recurrence relations are given by

$$\begin{aligned} xJ_p'(x) + pJ_p(x) &= xJ_{p-1}(x) \\ xJ_p'(x) - pJ_p(x) &= -xJ_{p+1}(x) \\ J_{p-1}(x) - J_{p+1}(x) &= 2J_p'(x) \\ J_{p-1}(x) + J_{p+1}(x) &= \frac{2p}{x}J_p(x). \end{aligned}$$

Similar formulas as above holds for Bessel functions of the second kind [15].

A.3 Spherical Bessel Functions

When inserting $p = n + \frac{1}{2}$ into equation (A.2.1) the Bessel function of the first kind of half an order integer is obtained

$$J_{n+\frac{1}{2}}(x) = (-1)^n x^{n+\frac{1}{2}} \left(\frac{d}{xdx}\right)^n \left\{x^{-\frac{1}{2}} J_{\frac{1}{2}}(x)\right\}. \tag{A.3.1}$$

The Bessel functions of second and third kind of half an order integer are obtained in the same way.

One application of the the Bessel functions of half an integer order are the spherical Bessel functions

$$\begin{aligned} j_n(x) &= \sqrt{\frac{\pi}{2x}} J_{n+\frac{1}{2}}(x), \qquad y_n(x) = \sqrt{\frac{\pi}{2x}} Y_{n+\frac{1}{2}}(x), \\ h_n^{(1)}(x) &= \sqrt{\frac{\pi}{2x}} H^{(1)}_{n+\frac{1}{2}}(x), \qquad h_n^{(2)}(x) = \sqrt{\frac{\pi}{2x}} H^{(2)}_{n+\frac{1}{2}}(x), \end{aligned} \tag{A.3.2}$$

where $J_{n+\frac{1}{2}}$ is the Bessel function of the first kind of half an integer order and $Y_{n+\frac{1}{2}}$ the Bessel function of the second kind of half an integer order. $H^{(1)}_{n+\frac{1}{2}}$ is the Hankel function of the first kind of half an order integer and $H^{(2)}_{n+\frac{1}{2}}$ is the Hankel function of the second kind of half an order integer.

A.3.1 Recurrence Relations

Recurrence relations are a convenient way of calculating the next term of a sequence. The following general recurrence relation can be used to compute the next term as a function of the preceding terms. If one of the spherical Bessel functions j_n, y_n, $h_n^{(1)}$ or $h_n^{(2)}$ are denoted by ψ_n, the recurrence relations follows [18]:

$$\begin{aligned} \psi_{n-1} + \psi_{n+1} &= \frac{2n+1}{x}\psi_n \\ n\psi_{n-1} - (n+1)\psi_{n+1} &= (2n+1)\frac{d\psi_n}{dx}. \end{aligned}$$

Appendix B

Mie Theory

This section is partly based on the book by Bohren and Huffman [5].

Gustav Mie considered a spherical particle in a medium. The refractive index for the particle is denoted by m and can be a complex number. This particle was then hit by an incident plane electromagnetic wave, i.e. infrared light. The light is then scattered, absorbed by the sphere or transmitted through the particle. The transmitted light is then detected by a detector on the other side of the particle. This is illustrated by figure B.1

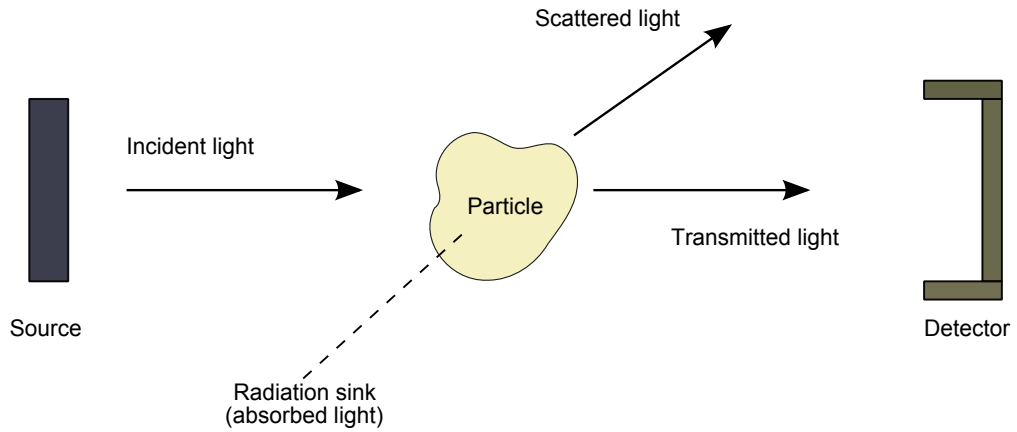

Figure B.1: Illustration of scattered light. The light is scattered, chemically absorbed by the object, and part of the incident light is transmitted to the detector.

Mie first started with an electromagnetic field $(\vec{E}, \vec{H})$. This field must satisfy the wave equation in a linear, isotropic, homogeneous medium

$$\nabla^2 \vec{E} + k^2 \vec{E} = 0, \qquad \nabla^2 \vec{H} + k^2 \vec{H} = 0.$$

The vector functions $\vec{M}$ and $\vec{N}$ are introduced. $\vec{M}$ is constructed with the scalar function ψ and arbitrary constant c

$$\vec{M} = \nabla \times (c\psi),$$

$\vec{N}$ is then constructed from $\vec{M}$. They both satisfy the vector wave equation, are divergence-free, the curl of $\vec{M}$ being proportional to $\vec{N}$ and vice versa. Since $\vec{M}$ satisfy the vector wave equation, ψ is a solution of the scalar wave equation. The scalar wave equation for ψ is then written in spherical polar coordinates.

Any function that satisfy the scalar wave equation in spherical coordinates may be expanded as infinite series in the functions

$$\psi_{emn} = \cos(m\phi)P_n^m(cos\theta)z_n(kr),$$
$$\psi_{omn} = \sin(m\phi)P_n^m(cos\theta)z_n(kr),$$

where z_n is any of the spherical Bessel functions given in appendix A and P are the associated Legendre polynomials where n and m are integers which satisfies the following condition $n \geq m \geq 0$.

The electromagnetic field is split into three parts:the incident electromagnetic field, $(\vec{E}_i, \vec{H}_i)$, scattered electromagnetic field, $(\vec{E}_s, \vec{H}_s)$ and the field inside the sphere, $(\vec{E}_1, \vec{H}_1)$. This is illustrated in figure B.2.

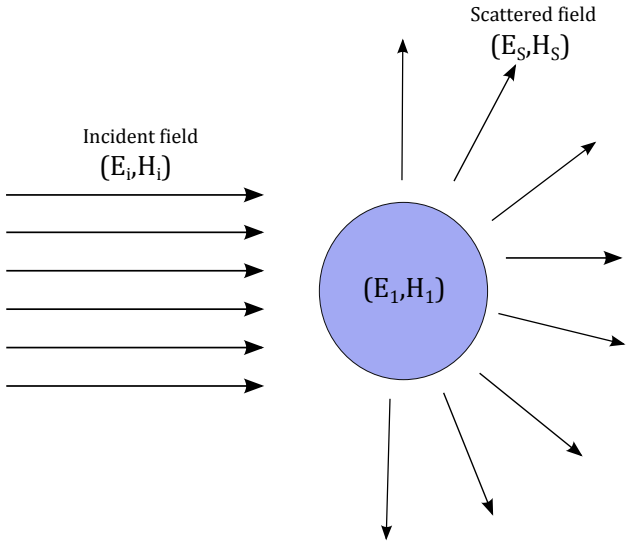

Figure B.2: Basic diagram showing the electromagnetic fields. The incident field $(\vec{E}_i, \vec{H}_i)$, the field inside the particle $(\vec{E}_1, \vec{H}_1)$ and the scattered field $(\vec{E}_s, \vec{H}_s)$.

$(\vec{E}_i, \vec{H}_i)$, $(\vec{E}_1, \vec{H}_1)$ and $(\vec{E}_s, \vec{H}_s)$ are expanded in an infinite series of vector spherical harmonics. The following boundary conditions are imposed on the

boundary

$$(\vec{E}_i + \vec{E}_s - \vec{E}_1) \times \vec{\hat{e}}_r = (\vec{H}_i + \vec{H}_s - \vec{H}_1) \times \vec{\hat{e}}_r = 0.$$

The incident, scattered and inside electromagnetic fields are then written as functions depending only on r, θ or ϕ. Four independent equations are needed to obtain expressions for the scattering coefficients. These equations are derived from the boundary conditions in component form. The coefficients for the field inside the particle follows

$$\left.\begin{aligned} \mathsf{c_n} &= \frac{\mu_1 j_n(x)[xh_n^{(1)}(x)]' - \mu_1 h_n^{(1)}(x)[xj_n(x)]'}{\mu_1 j_n(mx)[xh_n^{(1)}(x)]' - \mu h_n^{(1)}(x)[mxj_n(mx)]'} \\ \mathsf{d_n} &= \frac{\mu_1 m j_n(x)[xh_n^{(1)}(x)]' - \mu_1 m h_n^{(1)}(x)[xj_n(x)]'}{\mu m^2 j_n(mx)[xh_n^{(1)}(x)]' - \mu_1 h_n^{(1)}(x)[mxj_n(mx)]'} \end{aligned}\right\}, \tag{B.0.1}$$

The scattering coefficients

$$\left.\begin{aligned} \mathsf{a_n} &= \frac{\mu m^2 j_n(mx)[xj_n(x)]' - \mu_1 j_n(x)[mxj_n(mx)]'}{\mu m^2 j_n(mx)[xh_n^{(1)}(x)]' - \mu_1 h_n^{(1)}(x)[mxj_n(mx)]'} \\ \mathsf{b_n} &= \frac{\mu_1 j_n(mx)[xj_n(x)]' - \mu j_n(x)[mxj_n(mx)]'}{\mu_1 j_n(mx)[xh_n^{(1)}(x)]' - \mu h_n^{(1)}(x)[mxj_n(mx)]'} \end{aligned}\right\}, \tag{B.0.2}$$

where μ_1 is the permeability of the particle, μ is the permeability of the medium and m the refractive index. The size parameter x is given by

$$x = ka,$$

where a is the radius of the particle, k the angular wave number. The spherical Bessel functions are given in appendix A as

$$j_n(x) = \sqrt{\frac{\pi}{2x}} J_{n+\frac{1}{2}}(x), \qquad y_n(x) = \sqrt{\frac{\pi}{2x}} Y_{n+\frac{1}{2}}(x), \qquad h_n^{(1)}(x) = j_n(x) + iy_n(x), \tag{B.0.3}$$

where $J_{n+\frac{1}{2}}$ is the Bessel function of the first kind of half an integer order and $Y_{n+\frac{1}{2}}$ the Bessel function of the second kind of half an integer order given in appendix A.

The Riccati-Bessel functions

$$\psi_n(\rho) = \rho j_n(\rho), \qquad \xi_n(\rho) = \rho h_n^{(1)}(\rho), \tag{B.0.4}$$

are often used to simplify the scattering coefficients. ρ is a dimensionless variable introduced for simplification. When equation (B.0.4) is inserted into equation (B.0.2) with the assumption $\mu_1 = 1$, equation (B.0.2) transforms

$$\mathsf{a_n} = \frac{m\psi_n(mx)\psi_n'(x) - \psi_n(x)\psi_n'(mx)}{m\psi_n(mx)\xi_n'(x) - \xi_n(x)\psi_n'(mx)} \tag{B.0.5}$$

$$\mathsf{b_n} = \frac{\psi_n(mx)\psi_n'(x) - m\psi_n(x)\psi_n'(mx)}{\psi_n(mx)\xi_n'(x) - m\xi_n(x)\psi_n'(mx)}. \tag{B.0.6}$$

Appendix C

Tables

Table C.1: *Exact* is the dx calculated from the peaks of $\sum \mathsf{a_n}$ with resolution $\Delta\tilde{\nu} = 5\text{cm}^{-1}$, *Complicated formula* is the dx calculated using equation (2.9) and *Simple formula* is the dx calculated using equation (2.8). The results are generated with radius of the sphere $a = 5.5 \times 10^{-6}$m and refractive index $m = 1.48$. The results are calculated for $n = 12$ to $n = 57$

n	Exact $\sum a_n$	Simple formula	Complicated formula
12	0.742986662573985	0.759737884292489	0.738401590417633
13	0.760265422168731	0.759737884292489	0.735550727376339
14	0.777544181763474	0.759737884292489	0.733361689094409
15	0.760265422168729	0.759737884292489	0.73171890050505
16	0.742986662573987	0.759737884292489	0.73000398719042
17	0.760265422168731	0.759737884292489	0.728224775353495
18	0.742986662573985	0.759737884292489	0.726866110181915
19	0.742986662573987	0.759737884292489	0.725412478800909
20	0.742986662573987	0.759737884292489	0.724093155395408
21	0.725707902979241	0.759737884292489	0.722890345447984
22	0.742986662573987	0.759737884292489	0.721587409206597
23	0.725707902979241	0.759737884292489	0.720583281037179
24	0.742986662573987	0.759737884292489	0.719470094108727
25	0.725707902979241	0.759737884292489	0.718620408374767
26	0.725707902979241	0.759737884292489	0.717657378090542
27	0.725707902979241	0.759737884292489	0.716760746228436
28	0.725707902979241	0.759737884292489	0.715923873832521
29	0.777544181763474	0.759737884292489	0.715140978571176
30	0.760265422168732	0.759737884292489	0.714870095530547
31	0.760265422168729	0.759737884292489	0.714466826024848
32	0.777544181763474	0.759737884292489	0.714087889536861
33	0.760265422168729	0.759737884292489	0.713872172398262
34	0.760265422168729	0.759737884292489	0.71353185600432
35	0.760265422168732	0.759737884292489	0.713210362288491
36	0.760265422168729	0.759737884292489	0.712906171631232
37	0.345575191894877	0.759737884292489	0.712617923708834
38	0.39741147067911	0.759737884292489	0.709353988205688
39	0.760265422168729	0.759737884292489	0.706572958031983
40	0.742986662573987	0.759737884292489	0.706457800020092
41	0.742986662573987	0.759737884292489	0.706229611761016
42	0.760265422168729	0.759737884292489	0.706012010578516
43	0.742986662573983	0.759737884292489	0.705917616704036
44	0.74298666257399	0.759737884292489	0.705716644572234
45	0.742986662573983	0.759737884292489	0.70552438735005
46	0.742986662573983	0.759737884292489	0.705340290191967
47	0.639314105005525	0.759737884292489	0.705163844374251
48	0.760265422168729	0.759737884292489	0.704381261577724
49	0.760265422168736	0.759737884292489	0.70433109924677
50	0.777544181763467	0.759737884292489	0.704282929846151
51	0.74298666257399	0.759737884292489	0.704333066668552
52	0.777544181763474	0.759737884292489	0.704192112918369
53	0.777544181763474	0.759737884292489	0.704242096631132
54	0.742986662573983	0.759737884292489	0.704290215577588
55	0.760265422168729	0.759737884292489	0.704157700231082
56	0.760265422168729	0.759737884292489	0.704117748429769

Table C.2: Comparison of the obtained results using the exact dx from the positions of the first peaks of the single $\mathsf{a_n}$ with dx from the graph of $\sum \mathsf{a_n}$, dx calculated using the simple formula, equation (2.8), and the complicated formula, equation (2.9), which depends on x and n. All generated with radius of the sphere $a = 5.5 \times 10^{-6}$m and refractive index $m = 1.48$. The results are calculated for $n = 12$ to $n = 57$

n	Exact single a_n	Exact $\sum a_n$	Simple formula	Complicated formula
12	0.759737884292491	0.742986662573985	0.759737884292489	0.738241363461075
13	0.759737884292488	0.760265422168731	0.759737884292489	0.735704375304193
14	0.759737884292491	0.777544181763474	0.759737884292489	0.733497314598765
15	0.759737884292488	0.760265422168729	0.759737884292489	0.731559741057613
16	0.759737884292491	0.742986662573987	0.759737884292489	0.729845129869084
17	0.742437884292489	0.760265422168731	0.759737884292489	0.728317084363543
18	0.742437884292489	0.742986662573985	0.759737884292489	0.726707264753017
19	0.742437884292489	0.742986662573987	0.759737884292489	0.725253396088384
20	0.742437884292492	0.742986662573987	0.759737884292489	0.723933860530358
21	0.742437884292485	0.725707902979241	0.759737884292489	0.722730859824185
22	0.742437884292489	0.742986662573987	0.759737884292489	0.721629607300819
23	0.72513788429249	0.725707902979241	0.759737884292489	0.720617716684043
24	0.742437884292492	0.742986662573987	0.759737884292489	0.71949713066474
25	0.72513788429249	0.725707902979241	0.759737884292489	0.718640749998501
26	0.725137884292494	0.725707902979241	0.759737884292489	0.717671278348344
27	0.72513788429249	0.725707902979241	0.759737884292489	0.716768615613577
28	0.72513788429249	0.725707902979241	0.759737884292489	0.715926085030839
29	0.72513788429249	0.777544181763474	0.759737884292489	0.715137870936827
30	0.725137884292494	0.760265422168732	0.759737884292489	0.714398884270536
31	0.707837884292491	0.760265422168729	0.759737884292489	0.713704652523358
32	0.72513788429249	0.777544181763474	0.759737884292489	0.712904913590139
33	0.725137884292494	0.760265422168729	0.759737884292489	0.712292725240449
34	0.707837884292488	0.760265422168729	0.759737884292489	0.711714537837836
35	0.725137884292494	0.760265422168732	0.759737884292489	0.711032343766645
36	0.707837884292491	0.760265422168729	0.759737884292489	0.710517540016169
37	0.707837884292491	0.345575191894877	0.759737884292489	0.70990034995744
38	0.72513788429249	0.39741147067911	0.759737884292489	0.709313593732184
39	0.707837884292491	0.760265422168729	0.759737884292489	0.708878075822336
40	0.707837884292488	0.742986662573987	0.759737884292489	0.708343098655802
41	0.707837884292495	0.742986662573987	0.759737884292489	0.707832675688931
42	0.725137884292494	0.760265422168729	0.759737884292489	0.707345154219411
43	0.707837884292488	0.742986662573983	0.759737884292489	0.706991806241946
44	0.707837884292495	0.74298666257399	0.759737884292489	0.706543415722465
45	0.707837884292488	0.742986662573983	0.759737884292489	0.706113868662273
46	0.707837884292495	0.742986662573983	0.759737884292489	0.705702001578126
47	0.707837884292488	0.639314105005525	0.759737884292489	0.705306744847506
48	0.707837884292488	0.760265422168729	0.759737884292489	0.704927113430119
49	0.707837884292495	0.760265422168736	0.759737884292489	0.704562198668801
50	0.707837884292488	0.777544181763467	0.759737884292489	0.704211161026084
51	0.707837884292495	0.74298666257399	0.759737884292489	0.703873223634187
52	0.707837884292488	0.777544181763474	0.759737884292489	0.703547666554092
53	0.707837884292495	0.777544181763474	0.759737884292489	0.703233821654372
54	0.690537884292489	0.742986662573983	0.759737884292489	0.702931068033128
55	0.707837884292495	0.760265422168729	0.759737884292489	0.702548431945285
56	0.707837884292488	0.760265422168729	0.759737884292489	0.702267638653429

Table C.3: Comparison of the obtained results using the exact dx from the positions of the first peaks of the single $\mathsf{a_n}$ with dx calculated using the simple formula, equation (2.8), and the complicated formula, equation (2.9), which depends on x and n. All generated with radius of the sphere $a = 5.5 \times 10^{-6}$m and refractive index $m = 1.48$. The results are calculated for $n = 1$ to $n = 60$.

n	Exact single a_n	Simple formula	Complicated formula
1	0.589737884292489	0.759737884292489	0.94039112605591
2	0.569737884292489	0.759737884292489	0.87428183792493
3	0.559737884292489	0.759737884292489	0.831696298260981
4	0.63973788429249	0.759737884292489	0.801746817300063
5	0.689737884292489	0.759737884292489	0.782443801976631
6	0.729737884292489	0.759737884292489	0.769457093595324
7	0.73973788429249	0.759737884292489	0.760555283404514
8	0.759737884292488	0.759737884292489	0.753771448226654
9	0.759737884292489	0.759737884292489	0.74875941368064
10	0.759737884292489	0.759737884292489	0.74462866105812
11	0.769737884292489	0.759737884292489	0.741165472612259
12	0.759737884292491	0.759737884292489	0.738413440773525
13	0.759737884292488	0.759737884292489	0.735865770543534
14	0.759737884292491	0.759737884292489	0.733649261683107
15	0.749737884292488	0.759737884292489	0.731703274454572
16	0.759737884292489	0.759737884292489	0.729828313615521
17	0.749737884292491	0.759737884292489	0.728301108355446
18	0.739737884292493	0.759737884292489	0.726793121936531
19	0.74973788429249	0.759737884292489	0.725299726050788
20	0.739737884292492	0.759737884292489	0.72407072538613
21	0.739737884292481	0.759737884292489	0.72282934398221
22	0.729737884292486	0.759737884292489	0.721692702169434
23	0.739737884292492	0.759737884292489	0.720535598073398
24	0.72973788429249	0.759737884292489	0.71957631837013
25	0.729737884292494	0.759737884292489	0.718584205206148
26	0.719737884292488	0.759737884292489	0.717663178138581
27	0.729737884292494	0.759737884292489	0.716707830089712
28	0.72973788429249	0.759737884292489	0.715910885145337
29	0.719737884292492	0.759737884292489	0.715165512807392
30	0.719737884292488	0.759737884292489	0.714377411526921
31	0.719737884292496	0.759737884292489	0.713636831851063
32	0.719737884292488	0.759737884292489	0.712939600869085
33	0.719737884292492	0.759737884292489	0.712282020394082
34	0.719737884292492	0.759737884292489	0.711660801315903
35	0.70973788429249	0.759737884292489	0.711073008555451
36	0.719737884292492	0.759737884292489	0.710439730347285
37	0.70973788429249	0.759737884292489	0.709913009798812
38	0.719737884292492	0.759737884292489	0.709339785400804
39	0.70973788429249	0.759737884292489	0.708865282054504
40	0.70973788429249	0.759737884292489	0.708343793775497
41	0.709737884292494	0.759737884292489	0.707846278602641
42	0.709737884292487	0.759737884292489	0.707371120448959
43	0.709737884292494	0.759737884292489	0.70691684530639
44	0.709737884292494	0.759737884292489	0.706482105966701
45	0.709737884292487	0.759737884292489	0.706065668672761
46	0.709737884292494	0.759737884292489	0.705666401421489
47	0.709737884292487	0.759737884292489	0.705283263684847
48	0.709737884292494	0.759737884292489	0.704915297352289
49	0.709737884292494	0.759737884292489	0.704561618728587
50	0.699737884292489	0.759737884292489	0.704221411446312
51	0.709737884292487	0.759737884292489	0.703837977941892
52	0.709737884292494	0.759737884292489	0.703523479680338
53	0.699737884292489	0.759737884292489	0.703220314619298
54	0.709737884292494	0.759737884292489	0.702874754647129
55	0.699737884292489	0.759737884292489	0.702593374494573
56	0.709737884292494	0.759737884292489	0.702270209352965
57	0.699737884292489	0.759737884292489	0.702008412597081
58	0.699737884292496	0.759737884292489	0.70170547904024
59	0.709737884292487	0.759737884292489	0.701412317817917

Table C.4: Comparing the results obtained using the exact dx from the positions of the first peaks of the single $\mathsf{a_n}$ with dx calculated using the complicated formula, equation(2.9), which depends on x and n. The error is calculated between dx from the single $\mathsf{a_n}$ and from the complicated formula. All generated with radius of the sphere $a = 5.5 \times 10^{-6}$m and refractive index $m = 1.48$. The results are calculated for $n = 1$ to $n = 15$.

n	Exact single a_n	Complicated formula	Error
1	0.589737884292489	0.94039112605591	0.350653241763421
2	0.569737884292489	0.87428183792493	0.304543953632441
3	0.559737884292489	0.831696298260981	0.271958413968492
4	0.63973788429249	0.801746817300063	0.162008933007573
5	0.689737884292489	0.782443801976631	0.0927059176841424
6	0.729737884292489	0.769457093595324	0.0397192093028352
7	0.73973788429249	0.760555283404514	0.020817399112024
8	0.759737884292488	0.753771448226654	0.00596643606583469
9	0.759737884292489	0.74875941368064	0.0109784706118496
10	0.759737884292489	0.74462866105812	0.0151092232343691
11	0.769737884292489	0.741165472612259	0.0285724116802302
12	0.759737884292491	0.738413440773525	0.0213244435189663
13	0.759737884292488	0.735865770543534	0.0238721137489537
14	0.759737884292491	0.733649261683107	0.0260886226093837
15	0.749737884292488	0.731703274454572	0.0180346098379156

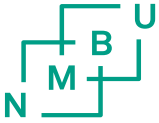

Norwegian University
of Life Sciences

Postboks 5003
NO-1432 Ås, Norway
+47 67 23 00 00
www.nmbu.no